Palaeogeography, Palaeoclimatology, Palaeoecology 637 (2024) 111985

Contents lists available at ScienceDirect

Palaeogeography, Palaeoclimatology, Palaeoecology

journal homepage: www.elsevier.com/locate/palaeo

Holocene savanna hydroclimate record from Kinrara Lake, north-east Queensland, Australia

Julie James [a], Rainy Comley [a], Christopher M. Wurster [a,c], Vladimir Levchenko [b], Patricia Gadd [b], Michael I. Bird [a,*]

[a] College of Science and Engineering, ARC Centre of Excellence of Australian Biodiversity and Heritage and Centre for Tropical Environmental and Sustainability Science, James Cook University, Cairns, QLD 4870, Australia
[b] Australian Nuclear Science and Technology Organisation (ANSTO), Locked Bag 2001, Kirrawee, DC, NSW 2232, Australia
[c] Isotrace NZ Ltd, 167 High St, Dunedin, New Zealand

ARTICLE INFO

Editor: P Hesse

Keywords:
Savanna
Stable isotope
Radiocarbon
Carbonate
Hydroclimate
ENSO

ABSTRACT

We present a record of hydroclimatic change over the Holocene from Kinrara Lake, in a seasonally dry savanna location in north-eastern Australia. The record is derived from the oxygen ($\delta^{18}O$) and carbon stable isotope ($\delta^{13}C$) composition of endogenic and biogenic (gastropod) carbonate. The stable isotope proxy records are complemented by elemental geochemical (Itrax) and sedimentological proxy data providing a record of hydrologic and climate change, spanning 10.5 ka to the present day. Two main forms of endogenic carbonate occur in the lake sediments; (i) carbonate associated with biofilms during the early-Holocene, under drier-than-modern conditions, (ii) photosynthetic and evaporatively-enriched precipitates in the late-Holocene, associated with enhanced climate variability inducing drought periods. Strong relationships between negative $\delta^{18}O$ values and increased Ti, Rb, Fe/Mn, inc/coh, are linked with strengthened monsoon conditions, while enhanced periods of dryness are inferred from more positive $\delta^{18}O$ values, increased Ca/$\sum$Fe, Ti, Al, and subsequent intensifications in lake productivity (higher Si/Ti, S/Ti, Mn/Ti). Three distinct phases can be identified in palaeohydrological history of the lake; (i) a relatively stable drier-than-modern phase during the early-Holocene (10.5 to 8.2 ka), (2) a significantly wetter-than-modern, monsoon-dominated phase through the mid-Holocene into the late-Holocene (8.2–2.8 cal yr BP), and (3) after 2.8 ka, increased intensity of ENSO-related rainfall variability during the late-Holocene, continuing into the present.

1. Introduction

North-eastern Australia lies adjacent to the western equatorial Pacific, in a region that is critical for the redistribution of energy and moisture within the Earths climate system. Convection within this region is driven by evaporation in the Indo-Pacific Warm Pool (IPWP), the region of largest heat energy transfer on the globe, vital for ocean-atmospheric convective transport from the equator to the poles (Krause et al., 2019). The climate of the region is currently subject to considerable inter-annual rainfall variability driven by a number of interacting phenomena including the El Niño-Southern Oscillation (ENSO) and the Inter-decadal Pacific Oscillation (IPO) to the east, the Indian Ocean Dipole (IOD) in the west, as well as the traverse of the Madden-Julian Oscillation (MJO) (Lough et al., 2014; Wheeler et al., 2009).

Inter-annual rainfall is modulated by latitudinal shifts in the position of the Inter-Tropical Convergence Zone (ITCZ) bringing warm moist air from the IPWP southwards into northern Australia (Reeves et al., 2013b), as part of the complex Australasian Monsoon System which in turn interacts with the East Asian summer monsoon and Indo-Australian Summer Monsoon (IASM) to the north (Krause et al., 2019). The modern climate of tropical Australia is dominated by the IASM. Therefore, tropical Australian paleoenvironmental data on centennial to millennial timescales is likely to dominantly reflect shifts in IASM intensity and position of the ITCZ, modulated by changes in the frequency, intensity and/or phase of shorter-term phenomena, likely dominated by ENSO, but including the influence of IPO, IOD, and MJO dynamics.

Understanding past hydroclimate variations across northern Australia provides critical information on timing and magnitude of monsoon variability on centennial to millennial timescales beyond the

* Corresponding author.
E-mail address: Michael.bird@jcu.edu.au (M.I. Bird).

https://doi.org/10.1016/j.palaeo.2023.111985
Received 11 May 2023; Received in revised form 30 November 2023; Accepted 14 December 2023
Available online 24 December 2023

relatively short instrumental record that is available. Such information assists in the identification of the drivers of IASM variability and the trajectory of regional hydroclimate change into the future. Local changes in IASM intensity are generally attributed to changes in the position of the ITCZ, in-turn related to millennial-scale changes in North Atlantic climate and meridional ocean circulation (decreased temperatures and/or increased ice cover resulting in southward ITCZ displacement (Denniston et al., 2013a; Griffiths et al., 2009; Griffiths et al., 2010; Lewis et al., 2010; Muller et al., 2012; Partin et al., 2007).

The most widely applied terrestrial proxy used to infer spatiotemporal changes in hydroclimate are time series changes in the $\delta^{18}O$ values of carbonate in speleothems (Denniston et al., 2013b; Krause et al., 2019). Low latitude speleothems record periods of intense monsoon rainfall as more negative $\delta^{18}O$ values can be linked to increased low-^{18}O monsoon-derived rainfall (Zwart et al., 2018; Bird et al., 2020). While shifts in the ITCZ have been linked to spatial changes in IASM rainfall distribution, changes in the strength of deep atmospheric convection generally has implications for total rainfall received and the $\delta^{18}O$ values of that rainfall (Krause et al., 2019). However, a time series of $\delta^{18}O$ values from calcite and aragonite in the Kimberly speleothem (KNI-51 - Denniston et al., 2013b), related IASM variability throughout the Holocene to changes in ENSO intensity in the later Holocene, rather than to the changes in the position of the ITCZ.

Late-Holocene ENSO intensification impacting the IASM has also been identified, with varying times of initiation, in a range of microfossil, elemental geochemical and humification studies in north Queensland (Burrows et al., 2016; Kershaw, 1976; Moss and Kershaw, 2000; Tibby and Haberle, 2007; Turney et al., 2004; Walker, 2007; Moss et al., 2012), in addition to one speleothem record from the Chillagoe cave system (Turney et al., 2006a) (Fig. 1). However, these studies, with the exception of the Witherspoon swamp pollen record of Moss et al. (2012) are biased toward the rainforest areas in north-eastern Queensland, due to a paucity of perennial lakes and lack of continuous speleothem archives in seasonally dry environments. Tropical savannas are located in regions characterised by high evaporation and a strong contrast in seasonal precipitation (Peel et al., 2007), resulting in

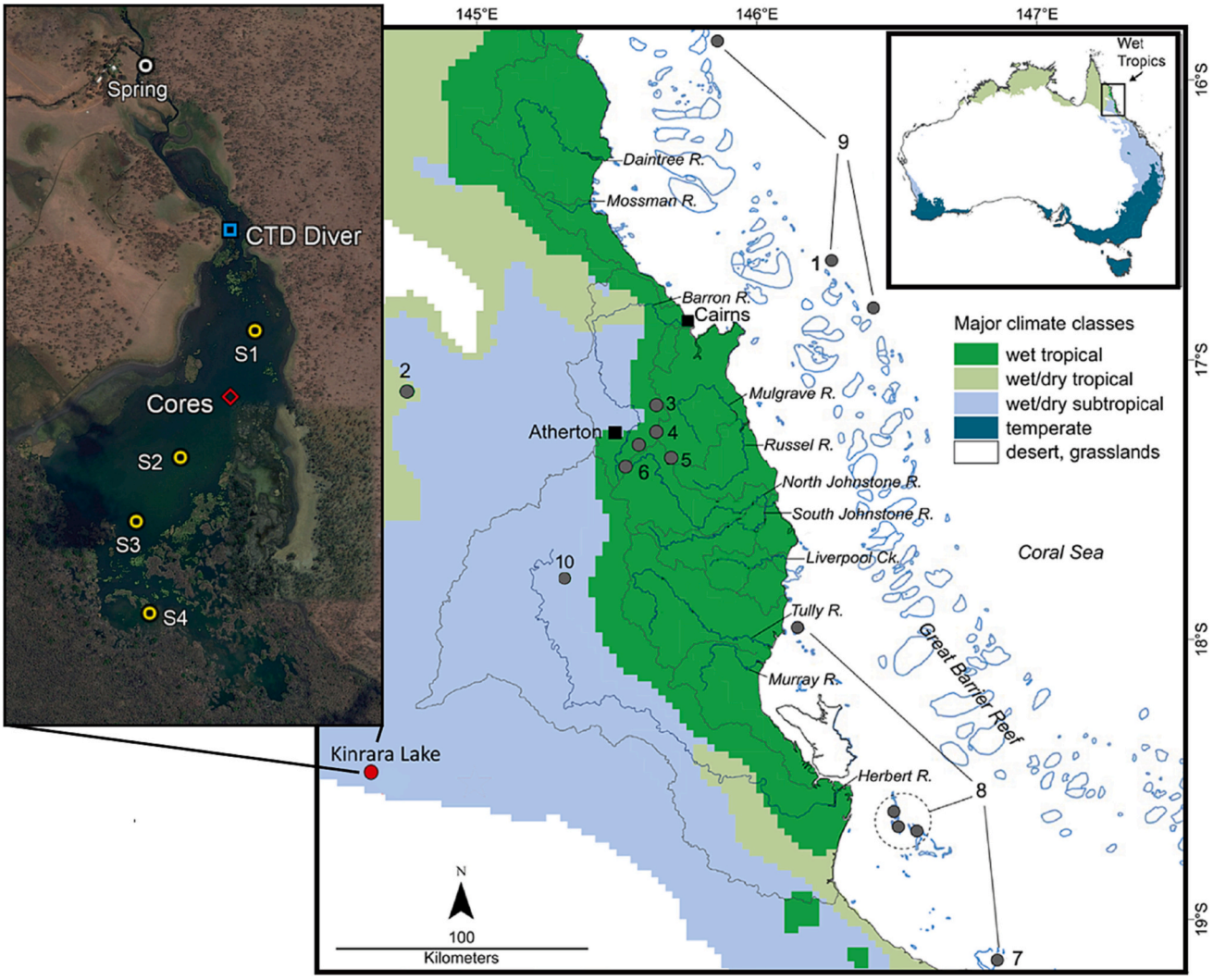

Fig. 1. Kinrara Lake study site (red marker) with reference to other palaeoenvionment studies in the region, modified from (Hughes and Croke, 2017). Sites are as follows: 1 – ODP820 (Moss and Kershaw, 2007); 2 – Chillagoe cave system (Haig et al., 2014; Turney et al., 2006a); 3 – Lake Euramoo (Haberle, 2005; Haberle et al., 2010; Tibby and Haberle, 2007); 4 – Lake Barrine (Walker, 2007; Li et al., 2022, 2023); 5 – Lynch's Crater (Muller et al., 2008; Turney et al., 2004; Turney et al., 2006b); 6 – Bromfield swamp (Burrows et al., 2016; Burrows et al., 2014); 7 – Magnetic Island (Lough et al., 2014); 8 – ENSO compilation sites (Donders et al., 2007); 9 – key Great Barrier Reef sea level sites (Lewis et al., 2013); 10 – Witherspoon Swamp (Moss et al., 2012). Satellite imagery from © 2018 Google Earth showing the water sampling sites (yellow and white circles), and CTD diver logger locality (blue square) used to characterize Kinrara Lake and spring with reference to the coring location (red diamond). Mapped using © 2019 Maxar Technologies imagery. (For interpretation of the references to colour in this figure legend, the reader is referred to the web version of this article.)

ephemeral lakes and therefore in non-continuous and/or degraded environmental archives (Bird et al., 2020).

No previous studies in northern Australia have examined lacustrine carbonates, which, like speleothems, can provide relatively direct information on hydroclimate as carbonates record the $\delta^{18}O$ value of precipitation, modified by fractionation effects related to the temperature of the lake water (Leng and Marshall, 2004; van Hardenbroek et al., 2018a). While biogenic carbonates (e.g. gastropods) are common in some lacustrine environments, their use as a paleoenvironmental proxy is complicated due to poorly constrained metabolic fractionations and often incomplete representation throughout lake sediment cores. As a result, when analysed, their use tends to be restricted to well-studied species, with demonstrated applications biased to the northern hemisphere (van Hardenbroek et al., 2018b). In lake sediment records, mollusc stable isotope compositions are often analysed in conjunction with endogenic carbonates, which precipitate in lake waters directly from the epilimnion or sediment water interface (Leng et al., 1999; Leng and Marshall, 2004; van Hardenbroek et al., 2018b). However, environmental controls coupled to a usual lack of carbonate influx from inorganic sources due to elemental mobility and through-flow lead to a lack of endogenic carbonates in a stratigraphically secure context in most northern Australian lacustrine settings.

Kinrara Lake, located in the seasonally dry interior region of tropical north Queensland (Köppen Climate Classification - Peel et al., 2007), is potentially unique in that it is not only a perennial lake, but intervals in the sedimentary record contain abundant gastropods and endogenic carbonates, providing access to isotopic information on Holocene hydroclimate. This lake therefore has considerable potential to yield a unique, high-resolution record of northern Australian hydroclimate over the Holocene. The principal aim of this study is to provide the first lacustrine carbonate isotope record of palaeohydrological change for tropical northern Australia. The record will provide centennial/millennial scale insight into the drivers of monsoon intensity and variability in a low latitude tropical savanna.

This study has the following objectives; (i) provide a comprehensive stratigraphic description of the sedimentary record of Kinara Lake (ii) develop a robust chronology for lake sediment accumulation and determine the time of lake genesis, (iii) identify the mineralogical composition and mode of deposition of endogenic carbonates within Kinrara Lake, (iv) develop a chronologically controlled record of changes in the stable isotopic composition of endogenic and biogenic (gastropod) carbonates, (v) complement the carbonate isotope record with other geochemical and sedimentological information from the sediment core, (vi) contrast results from Kinrara Lake with other paleoclimate proxies from the north-east Queensland, and (vii) identify the possible drivers of environmental change inferred from the record.

2. Study area

2.1. Geological setting and lake genesis

Kinrara Lake (18°30′4.43"S, 145°2′27.74″E, elevation 592 m – Fig. 1) is a spring-fed, basalt-dammed lake located in northeast Queensland on the weathered basalts of the McBride Volcanic Province (up to 3 Ma, Whitehead, 2010). Kinrara Lake was formed as a result of an eruption from the Kinrara Volcanic vent ~20 km NE damming springwaters and creek waters with basalt that flowed southeast into a pre-existing drainage channel toward the Burdekin River. Dating the complex 'a'ā and pahoehoe Kinrara basalt flows has been difficult (Cohen et al., 2017). Direct $^{40}Ar/^{39}Ar$ dating of Kinrara basalt has yielded a weighted mean age of 7 ± 2/2 ka (Cohen et al., 2017), noting that the flows sampled for dating in that study did not include the flow that dammed the lake.

2.2. Hydrology

Kinrara Lake is a small (~2.5 km^2), shallow open lake with an irregular perimeter. The catchment feeding the lake is gently sloping (<0.01°) and covers an area of ~111 km^2. Satellite imagery indicates that the lake surface area increases substantially during high rainfall wet seasons. However, due to the flat topography of the region, a doubling of lake area increases lake depth by only 1 m (maximum 2.8 m), at which point a sill is breached in the SE corner of the lake. While an ephemeral stream, Glenlofty Creek, runs into the lake along the basaltic drainage line, the major and perennial source of water is groundwater of the Upper Burdekin River Basin in the McBride Province. The lagoon is fed by Kinrara spring located ~2 km NNW of the lake (Fig. 2). The spring has been continually active since the Kinrara cattle property was established in the early 20th century, discharging bicarbonate-containing freshwater suitable for human and livestock consumption as well as irrigation. Average daily water temperatures from 2012 to 2019 in the Burdekin River headwaters (Valley of Lagoons gauging station - 120123 A), 18 km south of Kinrara Lake, are consistently stable at 24.7 ± 1 °C (Queensland Government, 2019).

2.3. Modern climate and vegetation

Regional temperature varies seasonally, with a mean minimum of 16.1 °C and a mean maximum 31 °C (Mount Surprise Township, 77 km NE from Kinrara Lake) with lowest temperatures in June–July and highest November–December based on data from 1873 to 1978 (BOM, 2019a). Rainfall in the region is highly variable with a mean annual rainfall of 759 mm subject to substantial inter-annual variability and with rainfall dominantly falling in the summer months (Craigs Pocket Station - 18°33′47.88"S, 144°59′21.12″E; 10 km SW of Kinrara Lake from 1968 to 2019;BOM, 2019b). Around 90% of the rainfall is associated with tropical depressions off the coast to the east (QPWS Enhanced Fire Managment Team, 2012). Currently, no information exists on the stable isotope composition of precipitation at the study location. However, daily rainfall isotope data over seven years are available for Cairns (Fig. 1) 250 km to the northeast. The data indicate that rainfall oxygen isotope composition varies widely from ~ − 5 to −10 ‰ during monsoon rain events, and ~ 0 to −3 ‰ associated with trade wind-derived rainfall (Munksgaard et al., 2019). Model estimates based on the Australian meteoric water line, location and altitude suggest average annual precipitation values at the site of −5.8‰ VSMOW for $\delta^{18}O$ (−34.9‰ VDPB) (Bowen, 2019). Seasonal changes in temperature and precipitation results in hot, humid summers and cooler, dry winters with the region being classified as a tropical savanna.

Kinrara Lake lies within the tropical savannas of the Einasleigh Uplands bioregion, characterised by open Eucalypt woodland with an extensive grass understory community (Department of Environment and Energy, 2019). The region primarily maintains its original vegetation cover of annual and perennial grasses along with *Eucalyptus* spp., Melaleuca spp., *Acacia* spp., and *Cypress* spp., and cattle grazing is the dominant landuse in the catchment and more widely (Cohen et al., 2017).

3. Materials and methods

3.1. Modern lake hydrochemistry

Water for modern calibration studies was collected in 50 mL sealable plastic containers for measurement of the stable isotope composition of both the water and dissolved inorganic carbon (DIC). Samples were collected pre-wet season (December 2019 and 2021) and post-wet seasonal (April 2019 and August 2011/2018) from the spring outflow and sites within the Lake (Fig. 1). Fig. 1 shows additional sites where water quality measurements (temperature, pH, specific electrical conductivity, total dissolved solids and turbidity) and analysis of major cations.

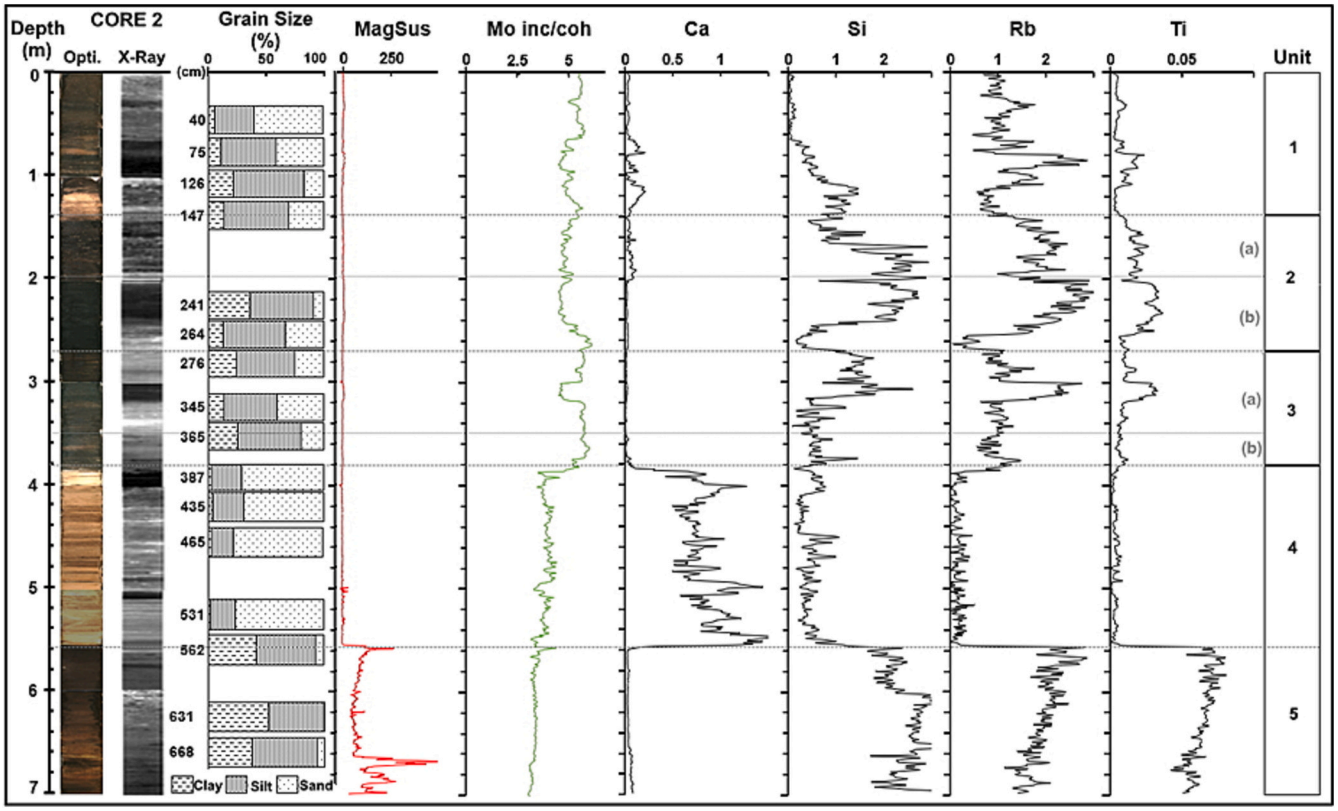

Fig. 2. Stratigraphic column for Core 2; optical image and x-ray scan, grainsize results (%) and depth sampled (cm), magnetic susceptibility (unitless) and ITRAX data (in raw counts per second) showing the 5 identified units (see SI - Section 2 for core description). Al, Si and Si represent raw counts x 1000.

Further information on collection and results for water are summarised in the Supplementary Information (SI - Section 1).

The water $\delta^{18}O$ values were measured using isotope ratio infrared spectroscopy via a Picarro L2130-i (Zwart et al., 2018) while dissolved inorganic carbon (DIC) and gastropod carbonate composition was analysed by acidification using the ThermoFinnigan Gasbench II coupled to a Thermo Delta Plus mass spectrometer. Refer to Sample Preparation - carbonate and dissolved inorganic carbon stable isotope analysis for details on instrumentation and technique.

3.2. Coring

Two cores were collected from locations a few metres apart in the deepest central part of the lagoon (18°30′4.428″S, 145°2′27.744″E – Fig. 1). Core 1 was collected in September 2010 to 4 m using a piston hand coring system from a floating platform. Core 2 was collected in October 2018 to 7 m using a hydraulic piston raft-mounted coring rig. Both cores were 5 cm in diameter and collected in 1 m plastic liners. Core 1 was described in the field and subsequently sub-sampled at 1 cm intervals, weighed and lyophilized for bulk density and archival purposes. Core 2 was frozen, halved in the laboratory, with one half kept for archival purposes and non-destructive geochemical analysis (i.e. ITRAX). The other half was sub-sampled every 2 cm using a drill press (diameter 1.9 cm), with samples weighed and dried for subsequent analytical work. Core 1 was correlated with Core 2 using a combination of stratigraphic boundaries including marker layers (e.g., shell dominated beds), radiocarbon ages of organic material, and stable isotopic data. All intervals from both cores were corrected to represent the 1 m interval recorded as cored in the field prior to analysis to create a master stratigraphy.

3.3. Stratigraphy and grain size analysis

Core 2 was subject to detailed description of stratigraphy focusing on the physical features (e.g. darkness, stratification, elasticity), colour, structure and visible components (origin of organic fragments, charcoal, gastropods). Unit boundaries were identified as distinct contacts between units of different colour and structure, with further support for boundaries derived from magnetic susceptibility, elemental profiles, gastropod abundance, stable isotope results and grain size analysis. A detailed stratigraphic description is provided in the SI – section 2.

The grain size distribution for 16 samples (2–3 samples per metre) from Core 2, was determined using a Malvern Mastersizer 2000 laser diffraction spectrophotometer. Samples were selected based on visual transitions in stratigraphy, magnetic susceptibility and μXRF results. Approximately 500 mg of sample was pretreated with 10–20 mL of 30% H_2O_2 to remove organic matter then ~10 mL of 2 N HCl to remove carbonates. Samples were then rinsed with ~500 mL deionized water to remove acidic ions and further treated with ~25 mL of 1 M NaOH to remove biogenic silica. The samples were then rinsed to neutralize the sediments before adding ~10 mL of 0.05 M of sodium hexametaphosphate and agitated to disperse the grains prior to laser analysis.

3.3.1. Chronology

Radiocarbon measurements from sixteen samples were obtained (see SI – Section 3); five samples selected from Core 1 (from 1 to 4 m), and eleven samples from Core 2 (4–7 m), using a marker bed at the 4 m interval to correlate between the two cores (see SI - Section 2). Two samples of bulk sediment and one sample of woody material were submitted for dating, both sample types subject to acid-base-acid pretreatment prior to combustion and graphitization. The remaining samples submitted for radiocarbon measurements were stable polycyclic aromatic carbon (SPAC) - the stable pyrogenic carbon fraction isolated using hydrogen pyrolysis (HyPy) (Ascough et al., 2009; Bird et al., 2014;

Wurster et al., 2012). Briefly, 1–3 cm^3 of sediment was pre-treated using 30% H_2O_2 overnight, to enhance removal of labile carbon (Orr et al., 2021), followed by 2 N HCl, to remove carbonates (Mishra et al., 2019), then filtered with ultrapure water until neutral. SPAC was separated from labile carbon via HyPy which involves heating up to ~600 °C assisted by high (>10 MPa) hydrogen pressures in the presence of a dispersed sulphided molybdenum catalyst (i.e. aqueous/methanol (1:1) solution of ammonium dioxydithiomolybdate [$(NH_4)_2MoO_2S_2$]) (Bird et al., 2015; Wurster et al., 2012). Hypy pre-treatment was conducted at James Cook Universitys Advanced Analytical Center (JCU-AAC) in Cairns. Other pre-treatment (acid-base-acid), combustion, graphitization, radiocarbon dating was conducted at either the Centre for Accelerator Science (CAS) at the Australian Nuclear Science Technology Organisation (ANSTO; prefix OZ) in Sydney or the Waikato Radiocarbon lab in New Zealand (prefix WK). Radiocarbon ages were calibrated with the SHCal20 calibration data set (Hogg et al., 2020) within the Bayesian age-depth modelling programme *rbacon* (Blaauw and Christen, 2011) which provides output as calibrated years before 1950 (Cal yr BP).

3.4. Sample preparation

3.4.1. Endogenic carbonates

A total of 175 samples were analysed from Core 1 (87 samples) and Core 2 (88 samples). Additionally, one modern sample of carbonate precipitating within the epilimnion was analysed. To separate the endogenic carbonates from the biogenic carbonates (i.e. gastropod shells) and other detrital material, samples were wet-sieved with distilled water using mesh sizes from 2000 μm to 63 μm. The fine fraction (<63 μm) was collected in a glass beaker and excess water decanted after centrifugation of the sediment. At this point samples were subdivided for additional analysis (e.g. XRD, SEM, TEM) and prepared accordingly.

3.4.2. Biogenic carbonates - gastropod shells

A total 158 gastropod shells were analysed from Core 1 (76 individuals) and Core 2 (82 individuals), in addition, two live individuals (*Melanoides tuberculata*) were collected from the lake. In total, 8 different species were identified throughout both cores, however, only two of the most common species were analysed in this study; *M. tuberculata*, including its conspecific morphotype formerly described as "*Thiara (Plotiopsis) balonnensis*" (Glaubrecht et al., 2009), and *Gyraulus gilberti*, all both species biomineralizing aragonite (Hallan, 2011; Shanahan et al., 2005). These two species were selected due to their dominance throughout the core, co-occurrence in a number of intervals, and single occurrence during periods of minimal biogenic input, to facilitate statistical analysis and accurate comparison throughout the core (Leng and Marshall, 2004). Shells were selected based on preservation, ability to identify to species, dominance within the layer and size (4–15 mm; mean 6 mm; *G. gilberti* maximum size is 5 mm). Generally, whole shells were used for stable isotope analysis, however, within 4 intervals of Core 2, only shell fragments were preserved and were used accordingly.

3.4.3. Carbonate stable isotope analysis

Stable isotope pre-treatment involved the oxidation of organic material from the endogenic carbonate fine fraction, modern shells and modern carbonates, using alkaline 18% H_2O_2 reagent (Falster et al., 2018). The solution was prepared by mixing 20 mL 0.5 M NaOH, 240 mL 30% H_2O_2 and 200 mL of ultrapure water. A 2 mL aliquot of the reagent was added to ~2 cm^3 (shell or 1 cm^3 modern carbonate) per sample and gently agitated every 15 mins for one hour in a 50 °C oven. After 1 h a further 2–4 mL of reagent was added, agitated and left to react in the oven overnight. After 24 h, each of the 10 mL vials were filled with distilled water and centrifuged. The supernatant fluid was decanted, the sample rinsed 3 times with distilled water and freeze-dried. Endogenic and biogenic carbonates (whole individual shells) were homogenised to a powder using an agate mortar and pestle prior to isotope analysis.

Carbon and oxygen isotope analyses were performed following a procedure similar to Breitenbach and Bernasconi (2011) using a ThermoFinnigan GasBench II equipped with a CTC Analytics autosampler coupled via a ConFlo IV interface and Delta V Plus mass spectrometer. For endogenic carbonates 100–3000 μg of powder (depending on carbonate content) was weighed into 12 mL (or 4 mL, if carbonate content was low) borosilicate glass exetainer vials to generate enough CO_2 for a reliable measurement. Biogenic carbonates and international reference materials required approximately 100 μg of pure carbonate. A total of 13 aliquots of international reference materials, NBS-18 and NBS-19, and Carrara marble were used within each analysis sequence (for a total of 46 samples per run), along with two blanks.

The vials were flushed with helium, reacted with 3–4 droplets of 100% orthophosphoric acid (H_3PO_4), manually injected using a syringe, to generate CO_2 gas and left to equilibrate at ~40 °C on the aluminium block of the autosampler for 16 h. Generated CO_2 was then measured for $\delta^{18}O$ and $\delta^{13}C$ values, with an uncertainty of ±0.1 ‰ or better. Sample measurements are reported in conventional delta notation with respect to V-PDB (Vienna Pee Dee Belemnite) and oxygen isotopes were corrected for phosphoric acid fraction using the Kim et al. (2007) temperature dependence equation (SI - Section 4). All isotope analyses were conducted at the Advanced Analytical Centre, James Cook University, Cairns.

3.4.4. Dissolved inorganic carbon (DIC) isotope analysis

Carbon isotope analysis for DIC was performed following a similar procedure as described above. The 6 mL of water was sampled using a filter syringe (0.2 μm PTFE membrane) directly from Kinrara Lake into a vial that was pre-flushed with helium. The samples were then stored at 4 °C and 6 mL of lake water was sampled directly into the vials at Kinrara Lake. The vials were then chilled until analysed. Samples were then reacted with 3–4 droplets of 100% H_3PO_4, to generate CO_2 gas and left to equilibrate at ~40 °C on the aluminium block of the autosampler for 16 h. Generated CO_2 was then measured for $\delta^{18}O$ and $\delta^{13}C$ values. Samples were run in batches of 25, including blanks (3 mL water), bicarbonate ($NaHCO_3$), NBS18 and LSVEC standards. Sample measurements are reported in conventional delta notation with respect to V-PDB with an uncertainty of ±0.1 ‰ or better.

3.4.5. Statistical analysis of isotope variation within mollusc shells

One-way analysis of variance (ANOVA) and *t*-tests (i.e. Tukeys-Kramer t-test for ANOVA and two-sampled t-test) were used to assess potential species-specific vital effects on $\delta^{18}O$ value (e.g. species-specific food or habitat preferences) in mollusc shells (Apolinarska et al., 2015), intra- or inter-species variation within sampled layers (1–2 cm intervals) and to validate the use of shell fragments in intervals where whole shells do not occur. Due to the uncertainties in phylogenetics and naming of *M. tuberculta*, *T. balonnensis*) were analysed as different species. No statistical significance was observed in either cores for assessed intervals, validating the use of both species (*M. tuberculata*/"*T. balonnensis*", and *G. gilberti*) and their fragments for paleoenvironment interpretation of $\delta^{18}O$ value (see SI – Section 5 for ANOVA tables and t-test summaries). Isotope results reflect mean stable isotope values for all analyses in a given interval.

3.4.6. ITRAX core scanning, X-radiographic, optical images and magnetic susceptibility

Core 2 was used to generate μXRF elemental profiles using the second-generation non-destructive ITRAX core scanner at the Institute of Environmental Research, ANSTO, Sydney. Operating conditions were 30 kV and 55 mA, step size of 1000 μm and 10 s count time. XRF data generated by ITRAX is in thousands of counts per second (cps) and requires normalisation to account for variations throughout the sediment associated with differing amounts of water content, organic matter, grain size and bulk density (Davies et al., 2015). To correct for interference, the elemental counts were divided by the Mo incoherent

integral (cps), as a Mo-tube X-ray source is used for XRF scanning, and reflect a ratio (Davies et al., 2015). All data was then smoothed using a 10-point running mean to reduce noise.

Initially, geochemical records of 38 elements were produced, reduced to a subset of useful elements (Ca, Fe, K, Mn, S, Si, Ti), elemental ratios including scattering; incoherent (inc, Compton scattering equivalent) and coherent (coh, Rayleigh scattering equivalent), indicative of lighter element scatter from C, O, H, which are useful for paleoenvironmental reconstruction. As Fe and Mn are both also lithogenic elements, they were normalised by Ti to remove influence of detrital input (Kylander et al., 2007; Moreno et al., 2007). As elements can play multiple roles depending on their individual chemistry and limnological conditions, choice of elements and elemental ratios was narrowed down based on the reliability of individual elemental profiles and by reference of other Holocene palaeolimnological studies from tropical latitudes or similar hydrological settings using the same geochemical μXRF proxies (see SI - Section 6 for discussion).

The ITRAX core scanner produced X-radiographic (45 kV and 55 mA with a step size of 1000 μm) and optical images. Radiographic images were positives, with higher density sediments appearing darker and lower density sediments appearing lighter (Croudace et al., 2006). A sensor also produced low-field magnetic susceptibility (κ) profile at 0.5 cm intervals for Core 2 which helps to distinguish different origins of magnetic minerals in lacustrine sediments (e.g. allogenic; fluvial or aeolian, endogenic precipitates or authigenic; reductive diagenesis or bacterial magnetosomes - Dearing, 1999).

3.4.7. Supplementary analyses

In addition to the techniques required for chronology development and environmental reconstruction, other techniques were used to provide accessory information on mineralogy and mineral morphology to assist in interpretation. This included X-ray diffraction (XRD) analysis of both powders and clay smears to provide information on carbonate mineralogy and scanning electron microscopy (SEM) in conjunction with energy-dispersive X-ray spectroscopy (EDS) to obtain information on carbonate and sulphide morphology. The methodologies used for these components are provided in SI – Section 8.

4. Results

4.1. Stratigraphy, μXRF and grain size

Five major units were identified in the sedimentary sequence for Kinrara Lake Core 2 (Fig. 2), summarised below and described in detail in the SI - Section 2. The upper 4 units are of sedimentary origin while the lower unit (Unit 5 is at least partly volcanogenic).

Unit 1 (depth from 0 to 147 cm) - The uppermost unit, is characterised by dark-grey and brown very fine sand and clays, rich in organics (visibly and also indicated by Mo incoherent/coherent scattering), shell macrofossils and endogenic carbonates.

Unit 2 (depth from 147 to 200 cm) - Greenish-black blocky silty mud, high in organics and split into sub-units (a) and (b). Sub-unit (a) is rich in shells (40% volume composition from 138 to 205 cm) and has endogenic carbonates. Sub-unit (b) does not contain biogenic or endogenic carbonates. The interval 245 cm to 267 cm is black, rich in organics and with the lowest Si, Ti and Rb measured throughout the core. From the base of sub-unit (b), Si, Rb and Ti counts increase in a stepwise pattern, X-ray images show dark bands of high-density sediments with low magnetic susceptibility (relative to Unit 5) indicating that the clastic component is not volcanogenic.

Unit 3 (depth from 200 to 380 cm) - Greenish-black silty mud and and split into two sub-units. Sub-unit (a) lacks any gastropods and ITRAX shows a distinct peak in Si, Rb and Ti from 300 to 330 cm with a related decrease in organic matter. From 330 cm endogenic carbonates are present and in sub-unit (b) gastropod shell fragments are present and endogenic carbonates are found throughout.

Unit 4 (depth from 380 to 560 cm) - Is a carbonate marl characterised by clear wavy and flat, thin, laminar carbonate layers, interbedded with very fine sands and organic matter (Fig. 3c-d). The top of this unit is marked by a 3 cm layer composed dominantly of gastropods and used as a marker bed for correlation between Core 1 and Core 2 (Fig. 3a-b). ITRAX shows elevated levels of Ca throughout the unit and relatively lower Si, Rb, and Ti. The base of this unit represents the base of the lacustrine sequence.

Unit 5 (depth from 560 to 700 cm) - The base of the core is characterised by sediments fining upwards from coarse sand-sized material, likely partly granite saprolite at the base to fine clays at the top. The unit has a very high magnetic susceptibility and high metal content potentially indicative of a partly volcanogenic origin of the unit (ash and debris), mixed with saprolitic material. Unit 5 pre-dates lake formation so is not suitable for palaeolimological interpretation and not considered further in this study.

4.1.1. Chronology

Results of samples radiocarbon dated are presented in Table S4. Two markedly old dates occurred in unit 4, which are attributed to contamination by geogenic graphite that formed a component of the ejecta from the Kinrara eruption(s). Two additional dates at 3.3 and 3.9 m were flagged by rBacon as outliers and excluded from consideration in developing the final age model which is presented in Fig. 4. The model suggests the initiation of the lake by damming by the Kinrara flow at 10,500 cal yr BP, with periods of comparatively rapid sedimentation occurring both before and after a period of slow organic-dominated sedimentation between 200 and 280 cm (~7500–2500 cal yr BP).

Initial attempts to date the sediments using gastropods indicated a very significant, and variable, hardwater effect, resulting from the addition of geogenic CO_2 into the lake water from the Kinrara Spring. As a result, a living gastropod returned an apparent age of 937 ± 27 yrs. BP (WK-51096) and a modern (but dead at collection) specimen returned an age of 1290 ± 35 yrs. BP (OZO-415). These dates are not included in Table 1 nor in the dates used to generate the age model presented in Fig. 4.

4.2. Geochemistry

4.2.1. Modern lake water and carbonate isotopic values

Modern water stable isotope values were constant for spring waters independent of season (~ − 7.7‰; Table S2). However, lake $\delta^{18}O$ values vary ±1.5 ‰ between wet and dry season, with dry season values more enriched in heavier isotopes, an indication of evaporative fractionation effects. It is also observed that within the lake there is a lateral gradient to increasing $\delta^{18}O$ values with distance from the spring, likely indicating mixing of spring waters with evaporated lagoon waters (SI – Section 1). Additionally, both spring and lake water $\delta^{18}O$ values are within the broad range of values known to be associated with regional rainfall (Zwart et al., 2018; Munksgaard et al., 2019).

Modern carbonate samples from biogenic and endogenic sources returned the same $\delta^{18}O$ values (~ − 9 ‰) irrespective of sampling time. The gastropod shell (*M. tuberculata*) is likely to reflect a 2 to 3-year average based on size (~2.5 cm; Vogler et al., 2012; Work and Mills, 2013) while the endogenic carbonate precipitation occurred over a maximum period of 10 months (based on the time that the CTD logger on which the carbonate was precipitated had been deployed in the lake waters). Temperature fractionation equations (Dettman et al., 1999; SI – Section 3) for aragonite, using average $\delta^{18}O$ wet season values (−7.8 ‰ VSMOW), yield values of ~27 °C, equivalent to measured modern average temperatures, highlighting the modern precipitation is in isotopic equilibrium. $\delta^{13}C$ values for biogenic and endogenic carbonate samples diverged by ±3 ‰ and were higher than water dissolved inorganic carbon ($\delta^{13}C_{DIC}$) sampled from the spring and more similar to lake water values.

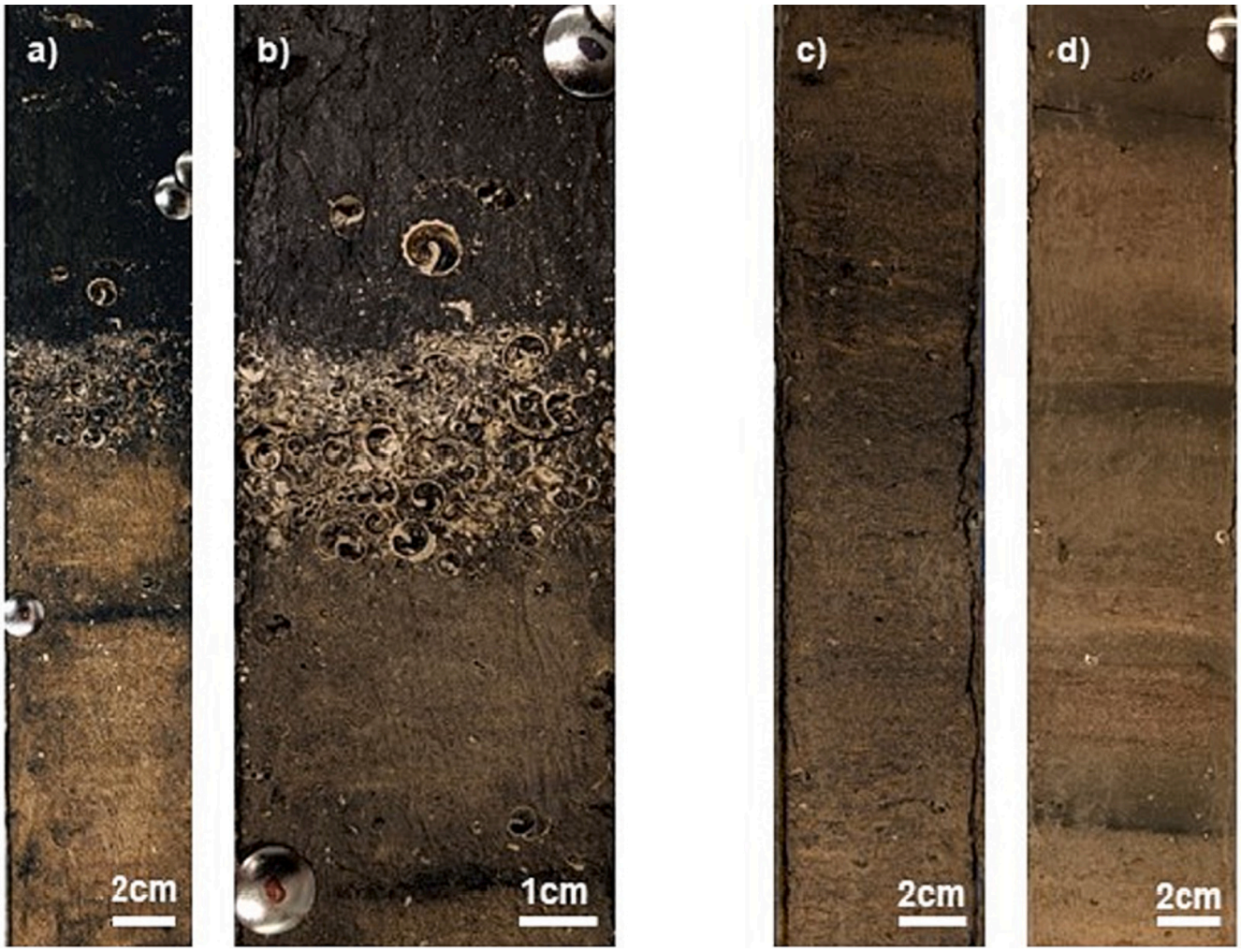

Fig. 3. Core images of Unit 4 carbonate marl; shell layer marker bed (a) and close up (b) at 384-387 cm, (c) wavy, organic rich laminae at ~500 cm, (d) flat laminae at 545 cm.

4.2.2. *Lake sediment carbonate stable isotope composition*

The sedimentary carbonate stable isotope record is incomplete, for both endogenic and biogenic aragonite, with all results presented in Fig. 5. This is due to the lack of significant carbonate precipitation between 7499 and 2742 cal yr BP. However, two brief periods of aragonite formation occurred around 7702 and 6944 cal yr BP producing both biogenic and endogenic carbonates. The biogenic aragonite record initiates at 10660 cal yr BP and the endogenic aragonite record begins 290 yrs. later (10,370 cal yr BP). Where cores 1 and 2 overlap, the cores also show similar isotope trends in that they both exhibit more positive and relatively stable values during the early-Holocene (~10,700 to 8200 cal yr BP) followed by abrupt decline to more negative values into the early-Holocene (8200 to 4200 cal yr BP) with values decreasing further into the late-Holocene (2600 cal yr BP to present) and exhibiting higher variability during these periods (Fig. 5).

Average isotope values and standard deviations for endogenic ($\delta^{18}O_{endo}$, $\delta^{13}C_{endo}$) and gastropods ($\delta^{18}O_{bio}$, $\delta^{13}C_{bio}$) summarised in Table 1, and all data is available in Table S5 and S6. One outlier value for $\delta^{13}C_{endo}$ (+3.4 ‰) is potentially associated with intense volcanic degassing (Italiano et al., 2014; Votava et al., 2017) was identified at the base of the Core 2, at 10480 cal yr BP and was not included in the descriptive statistics.

While $\delta^{18}O_{endo}$ and $\delta^{18}O_{bio}$ values showed minimal variation (Fig. 5), values for $\delta^{13}C_{bio}$ exhibited a clear vital effect (Leng and Marshall, 2004), with relatively lower $\delta^{13}C_{bio}$ compared to $\delta^{13}C_{endo}$. The offset ranged from 1.6 to 10.3 ‰ (mean − 6 ‰) between $\delta^{13}C_{endo}$ and $\delta^{13}C_{bio}$ (Fig. 10). Despite $\delta^{13}C$ values exhibiting the same overall trends, consistent differences in vital effects and clear offset relationships could not be distinguished from the available results, and this did not allow systematic corrections to be applied to the endogenic carbonate data. Therefore, only $\delta^{13}C_{endo}$ was used for paleoenvironmental reconstruction in the following sections.

In contrast, offsets between $\delta^{18}O_{endo}$ and $\delta^{18}O_{bio}$ values ranged from 0 to +3.9‰ (mean 0.4 ‰). The largest offsets were restricted to the Mid- to late-Holocene with $\delta^{13}C_{bio}$ becoming consistently more enriched in ^{18}O (mean $\delta^{13}C_{bio}$ = +1.8 ‰). As this trend was not seen consistently throughout, it is likely that the difference is not due to vital offsets, but changes in environmental conditions.

4.2.3. *Element ratios*

Like the isotope data, elemental (ITRAX) data (Fig. 6) shows a clear distinction between early-Holocene and Mid- to late-Holocene sediments. Additionally, the ITRAX data provides insight into periods where there is little or no carbonate precipitation (between 7900 and 2900 cal yr BP – Fig. 9). This period corresponds with changes in the elemental geochemical record with a decrease in Ti (only slightly for the at 8100 cal yr BP followed by a rapid increase from 6900 cal yr BP, which is maintained until 3000 yrs), During the 6900 yr event, Fe/Mn reduces and Mn/Ti ratios increases, highlighting a change to more oxidising conditions.

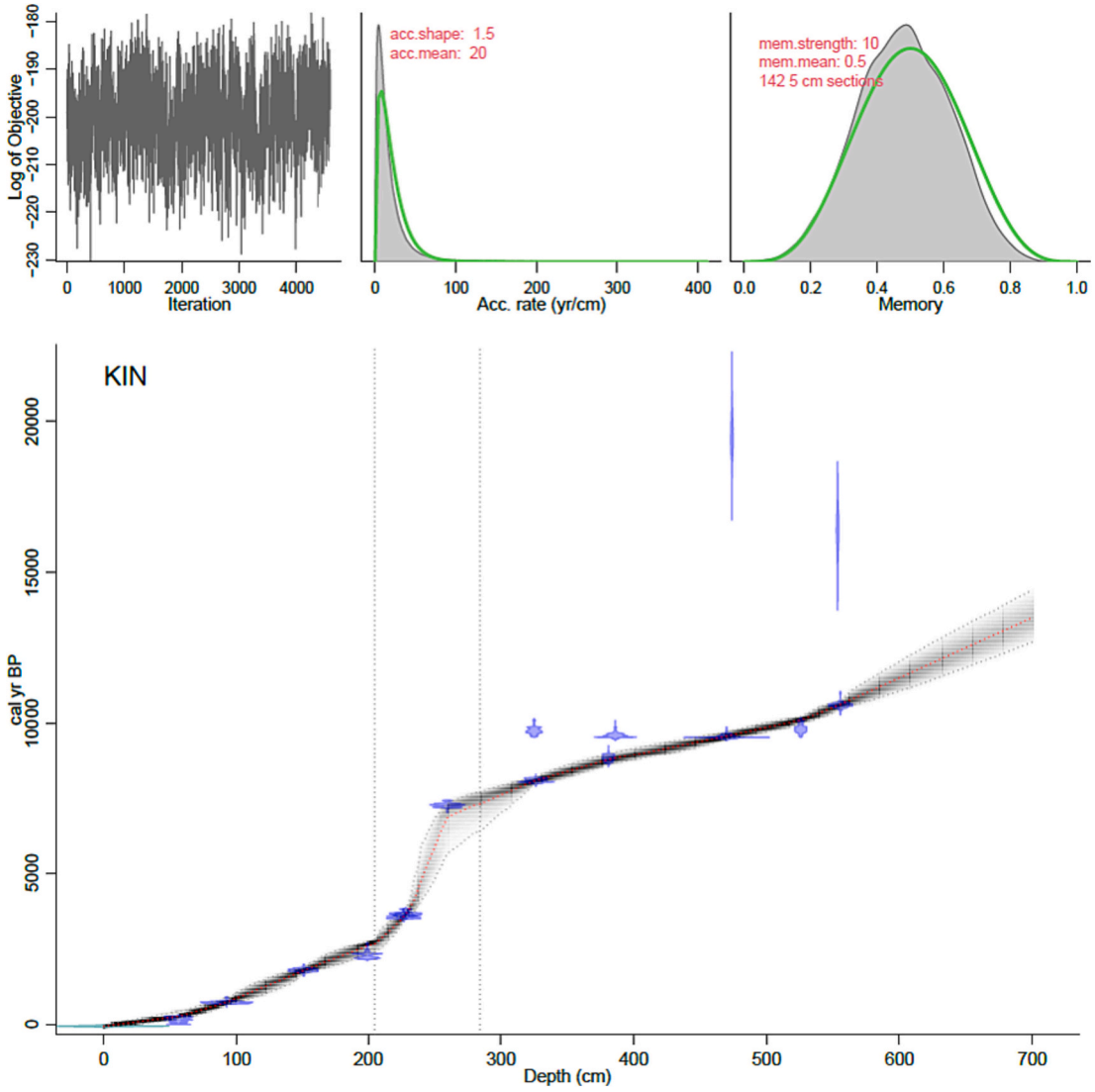

Fig. 4. rBacon age depth model for the Kinrara Lake composite record (see Table S4 for the dates used to construct the age model.

Table 1
Mean isotope values of carbonates in the Kinrara Lake cores with their associated standard error and sample size (n). Bold represents the average of both cores. All results are presented in Tables S5 and S6.

PERIOD	Core	$\delta^{18}O_{endo}$ (‰ VPDB)	$\delta^{18}O_{bio}$ (‰ VPDB)	$\delta^{13}C_{endo}$ (‰ VPDB)	$\delta^{13}C_{bio}$ (‰ VPDB)
early-Holocene (>8200 cal yr BP)	1	−6.9 (0.1) ($n = 6$)	−7.5 (0.1) ($n = 12$)	−5.8 (0.1) ($n = 6$)	−13.1 (0.3) ($n = 12$)
	2	−6.6 (0.1) ($n = 35$)	−7.7 (0.1) ($n = 31$)	−6.6 (0.2) ($n = 35$)	−13.8 (0.3) ($n = 31$)
	1 & 2	**−6.8 (0.1) ($n = 41$)**	**−7.6 (0.1) ($n = 43$)**	**−5.9 (0.1) ($n = 41$)**	**−13.3 (0.2) ($n = 43$)**
Mid to late-Holocene (<8200 cal yr BP)	1	−9.4 (0.9) ($n = 39$)	−8.6 (0.1) ($n = 25$)	−10.3 (0.1) ($n = 39$)	−16.4 (0.3) ($n = 25$)
	2	−10.3 (0.2) ($n = 24$)	−8.6 (0.1) ($n = 30$)	−10.9 (0.1) ($n = 24$)	−15.9 (0.3) ($n = 30$)
	1 & 2	**−9.8 (0.1) ($n = 63$)**	**−8.5 (0.1) ($n = 55$)**	**−10.5 (0.1) ($n = 41$)**	**−16.1 (0.2) ($n = 43$)**

Table S10 shows the correlation between lithogenic elements (Ti, Rh, Mn, Fe, Si) and other elements (S, Ca) used for paleoenvironment proxies and excluding the values in volcanogenic Unit 5. High correlations between Ti, Rb, Fe and Si, suggest a lithogenic origin for these elements, however, Al is input from, or generated by, another unrelated source. Elemental ratios of Ca/$\sum$ Fe, Ti, Al, Mn/Ti and Si/Ti all increase as isotope values increase (predominantly during the late-Holocene period), while Fe/Mn, Inc./Coh and elemental Ti decrease, resulting in inverse correlations between the two time periods (Fig. 6). During the period of no carbonate precipitation (Unit 3), metals associated with increased detrital input (i.e. run-off) increase; Si, Ti and Rb, along with a high Fe/Mn ratio and Inc./Coh (organic matter) associated with reducing conditions. Ti, Fe/Mn and Inc./coh also show more variability toward the end of the late-Holocene (~2900 cal yr BP).

4.2.4. *Mineralogy and petrography*

Powdered and clay smear XRD samples from Units 2 and 4 displayed clear 2θ XRD peaks corresponding to aragonite (see SI - Section 9), with no other crystalline carbonate polymorphs evident. SEM-EDS was used to confirm elemental composition of aragonite polymorphs with a dominance of Ca, O, and C in spectral signatures (see SI– Section 9).

SEM-EDS within Units 1 and 4 highlighted a range of primary aragonitic crystal habits and textures which varied within and between

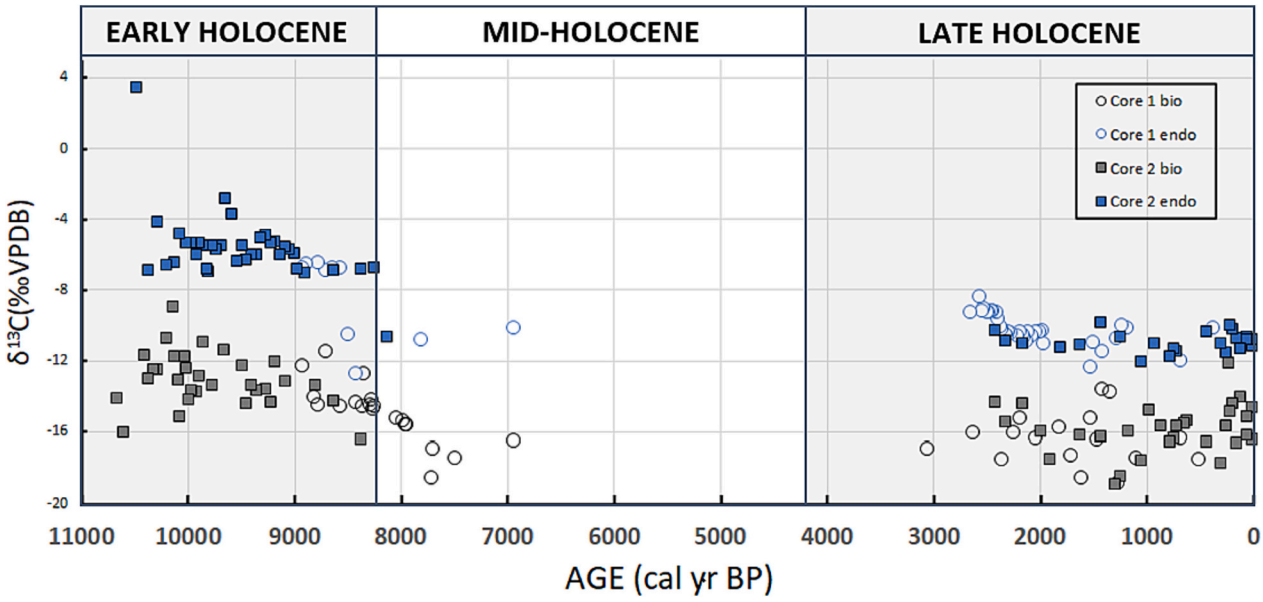

Fig. 5. $\delta^{13}C$ values for endogenic and biogenic carbonates for both Kinrara Lake cores.

samples. The most prevalent aragonitic crystalline forms varied between units; Unit 4 samples displayed a range of microbially mediated fabrics and chemically precipitated euhedral aggregates (Fig. S6 and S7), while Unit 1 samples were dominated by aragonitic euhedral rhomboid needles to lamellar matrix, binding silicate diatoms, organic materials and cubic pyrite. Unit 4 also exhibited high pyrite abundance as framboids (Fig. S8).

The most common form of aragonite in Unit 4 is elongate tightly packed acicular needles, lamellar blades and plates, forming spherical to ellipsoidal bundles ~2–8 μm in diameter (Fig. S9). The surfaces of these radiating forms are composed of nanocrystals elongated along the main axis of the bundle. Broken bundles display a hollow (central lumen, ~0.8 μm) from which needles often radiate. Aragonitic bundles are embedded within a larger, though similarly shaped, spherical to ellipsoid aggregates (~100–150 μm), along with silicate diatoms, bound together by an aragonite matrix. The aragonite crystals within the matrix ranged from euhedral aragonite rhomboid needles to lamellar aragonitic sheets (<15 μm). SEM images of Unit 4 highlighted smooth discoid polymorph of aragonite co-occurring in this interval (Fig. S7).

Aragonite crystals in Unit 1 were difficult to identify due to a high density of diatoms held in a matrix of what appeared to be organic microfibers (potentially cellulose which has similar appearance in alkaline conditions - Wolfe et al., 2002) (Fig. S9). Nonetheless, rhomboidal needles, lamellar plates and spherical to ellipsoidal aragonite bundles, similar to Unit 4, were identified (Fig. S9). Relatively large hollows (8–10 μm diameter) were also found, however, no crystals were radiating around them, described as Mode 2 formation of endogenic carbonate.

5. Discussion

5.1. Endogenic carbonate origins

Two main modes of endogenic carbonate precipitation are present in the Kinrara Lake record. Mode 1 (Unit 4) is dominated by cyanobacterial accretion of aragonite due to evaporative concentration of DIC during the early-Holocene, while mode 2 (dominantly in Unit 1 - Fig. 2) appears to be generated in complex benthic aragonite-precipitating biofilms, occurring shortly after lake genesis extending into the late-Holocene. The aragonite structures observed in the sediments are most similar to microbially mediated aragonite precipitates described in Oligocene Sarlieve Lake France (Bréhéret et al., 2008), and modern-Holocene deposits in freshwater Lake Bacalar, Mexico (Gischler et al., 2008).

Both mode 1 and 2 microbial textures are characterised by a hollow structure within which unicellular algae or cyanobacteria existed, acting as a nucleating surface for precipitation of small (<8 μm) aragonitic needles. However, benthic biofilms exhibit a coalescence of hollowed bundles (Bréhéret et al., 2008), often co-occurring with sulphate reducing bacteria (SRB) pyrite framboids (Fig. S8) which are commonly interpreted as a biomarker for biofilms and cyanobacterial mats (MacLean et al., 2008; Popa et al., 2004; Rozanov et al., 2007; Westall and Rincé, 1994).

Mode 1 microbially-mediated precipitates occur during photosynthesis, as a supersaturated microenvironment (high pH and supersaturated Ca^{2+}) develops around the cell causing carbonate to precipitate as CO_2 is drawn down (Schultze-Lam et al., 1997). This process can lead to seasonal 'whitings' as a consequence, as cyanobacteria blooms occur during seasonal growth, corresponding with periods of high productivity (Thompson and Ferris, 1990; Thompson, 2000). In Laguna Bacalar, precipitation occurs along filaments of Homeothrix and Leptolyngbya cyanobateria, and is enhanced by diatom photosynthesis causing further carbonate precipitation (Gischler et al., 2008). In Kinrara Lake, diatoms were also present during periods of endogenic carbonate precipitation. In addition, small individual needles of aragonite are also present (granular, blocky, lenticular and prismatic idiomorphic, generally <10 μm in size – Fig. S9) indicating abiotic precipitation through evaporative concentration (Fan et al., 2018).

Mode 2, coalescent biofilm fabrics, were the most common aragonitic texture identified in Unit 4, however, the exact mode of formation is unknown (Bréhéret et al., 2008). The presence of coalescent microspheres composed of radiating nanocrystals, suggests a benthic origin, which is further supported by the observation that aragonite presence was associated with other organically induced precipitates such as pyritic framboids formed by SRB (Fig. S8), and smooth discoid aragonitic precipitates (Fig. S7).

Mechanisms for carbonate production in microbial biofilms are quite complex and often biased toward dolomitic precipitates (Corzo et al., 2005; Dupraz et al., 2004; Tanner, 2010; Wright, 1999). Carbonate formation associated with biofilms generally occurs within microbial extracellular polymeric substances (EPS), essentially as by-products of microbial activity and EPS degradation, subsequent to the activity of SRB (Tanner, 2010). The presence of discoid aragonite aggregates

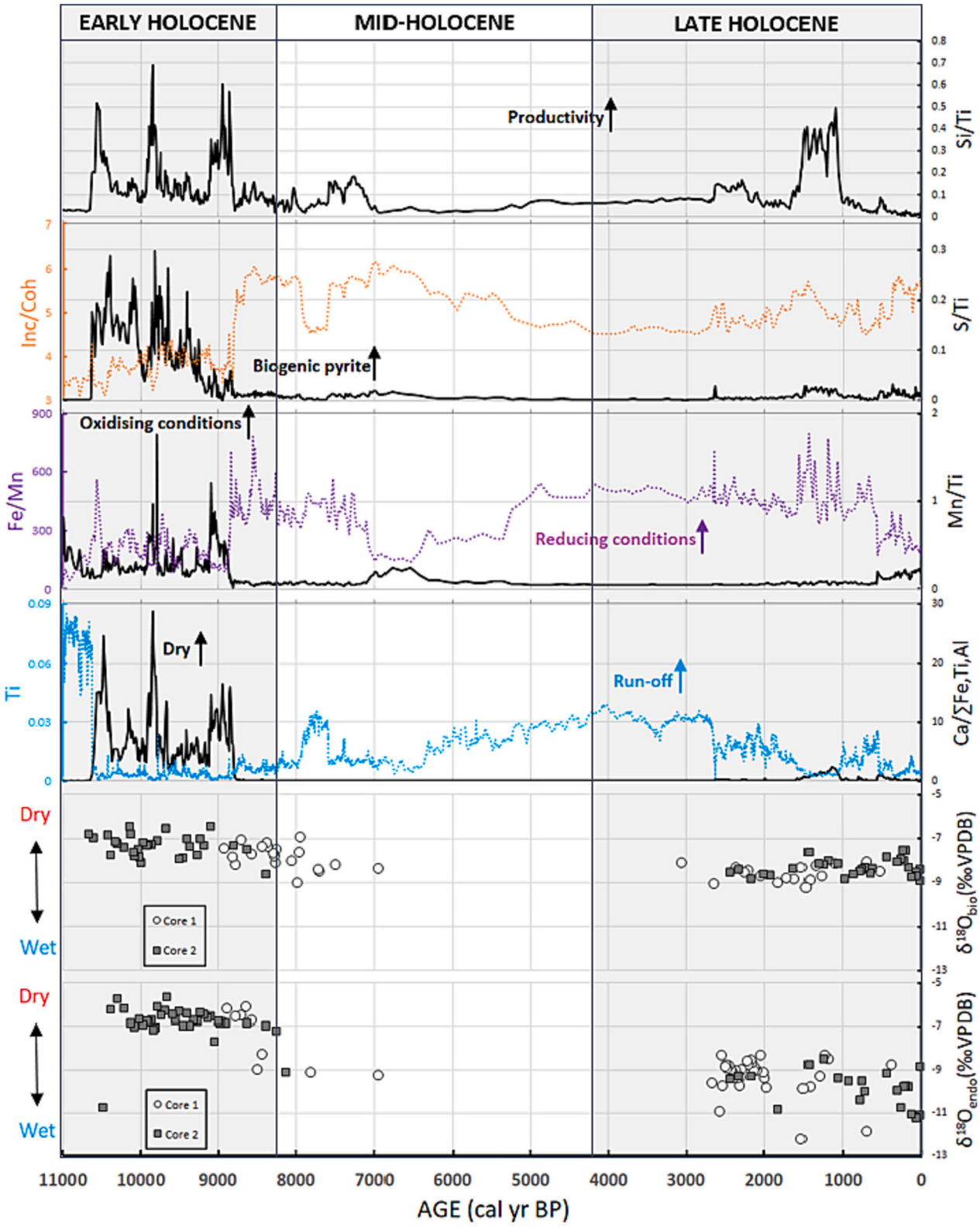

Fig. 6. Kinrara geochemical record over time. Geochemical proxies and stable isotope data (both cores) and their associated interpretation. For further information on the interpretation of elemental proxies of lacustrine relevance is also outlined in Table S9.

suggests an association with EPS degradation, as within a protein-polysaccharide organic matrix (Cheng et al., 2008; Eastoe and Dettman, 2016). This has not previously been described in sedimentary carbonates, therefore it is unclear what factors might favour the discoid structure over co-occurring coalescent bundles. However, the presence of hollow lumen forming nucleating surfaces suggests microalgae or bacteria within the biofilm (Bréhéret et al., 2008).

The presence of diatoms in the samples also indicates that reducing conditions supporting SRB metabolism were restricted to the sediment-water interface and eplimnetic conditions were still oxic. Therefore, a

contribution from eplimnetic cyanobacteria and algae is likely, however, the amount of carbonate produced from this source is unknown.

While aragonite formation does occur in other freshwater settings (McCormack et al., 2019), it is a rare phenomenon and it is not uncommon for other mineral polymorphs such as Mg-calcites and calcite to co-occur. Given the modern Mg/Ca from springwaters at Kinrara is ~3 (Table S1), and aragonite generally forms if the ratio is <5 (Bréhéret et al., 2008), higher resolution XRD analysis should be conducted to determine the dominant morphotype during periods of heightened monsoon activity (Unit 2).

5.2. Elemental geochemistry as a paleolimnological proxy

Paleoenvironmental interpretation of elemental data in lake sediments assumes that the lake sediment originates from external (allogenic) and/or internal (endogenic or authigenic) processes that deliver mineral and organic material to the lake floor. Elements such as Al, Ti and Rb are generally considered allogenic, as they are commonly associated with lithogenic detrital flux (Boës et al., 2011). Fe and Si are also lithogenic, however, they can be derived from other in situ lake processes. Precipitation of Fe can occur from lake water with changes of redox conditions and authigenic processes (Haberzettl et al., 2005), whereas Si can be biogenically precipitated (e.g. diatom tests) during periods of high productivity or when environmental conditions change to favour their preservation (Moreno et al., 2007). Similarly, Ca, can be either deposited endogenically (microbially mediated or chemically precipitated) or allogenically (weathering limestone or dolomite catchments) (Mueller et al., 2009). Therefore, displaying these data as a ratio over a known lithogenic allogenic component provides a more robust tool from which to derive insight into internal lake processes. Strong correlation ($r^2 > 0.5$) of lithogenic elements (Ti, Rb, Fe, Si, Mn) highlights a predominantly lithogenic origin for these elements in this record (Table S9). As Ti is the most widely used proxy for erosion and transport of silt and fine sand (Davies et al., 2015), it was selected as the major detrital component for elemental ratio analysis. High detrital inputs are evident during the mid-Holocene and into the late-Holocene (to 2.8 ka) indicating erosion and deposition at times of either more seasonally intense rainfall or reduced vegetation cover.

Fe and Mn profiles generally provide information about changing redox conditions (Davison, 1993). Higher Fe/Mn ratios are associated with anaerobic conditions, as Mn is more readily soluble than Fe in reducing conditions. Environmental factors that promote reducing conditions are those that obstruct mixing of oxygenated waters to the sediment-water interface causing thermal and chemical stratification (Boyle, 2002). A shift to higher Fe/Mn therefore may indicate changes in depth linked to enhanced stratification, or to de-oxygenation from organic decay following enhanced biological productivity linked to changing nutrient inputs (eutrophication) (Davies et al., 2015).

As Kinrara Lake can only attain a maximum depth of ~2.8 m before overflowing, major changes in redox conditions are unlikely to be associated with depth stratification alone. Therefore, periods of enhanced reducing conditions are more likely periods of higher organic input (coh/inc) resulting in eutrophication and/or increased productivity (Si/Ti) combined with high terrigenous input (Ti, Rb), (Fig. 6) which promote anoxic respiration and organic decay. Periods with relatively high oxidation (Mn/Ti) and reduction occur simultaneously during the late Pleistocene and early-Holocene suggesting chemical stratification. These periods are also associated with the presence of sulphate-reducing bacteria and biofilms (high Ca/∑Fe, Ti, Al) which thrive in reducing environments, and also high Si/Ti indicating biogenic silica, in turn suggesting increased productivity. These indicators in combination indicate chemical stratification is likely associated with periods of eutrophication.

Conditions promoting chemical stratification, oxic surface waters and eutrophic sediment conditions generally manifest vertically, due to seasonal changes (i.e. warm summer productivity) or natural diel cycling of dissolved oxygen in shallow bodies of water with photosynthesis-induced supersaturation during the day, changing to near anoxic during the night due to respiration (Diaz and Breitburg, 2009). However, lateral stratification can also occur, particularly in shallow dendritic reservoirs, influenced predominantly by one inlet water source (Diaz and Breitburg, 2009; Thornton, 1990). Anoxic zones tend to form downstream of lake inlets as waters are isolated from aeration by, for example, overgrowth of macrophytes and algae on the water surface. Once an anoxic zone forms in this system, it shifts laterally depending on input/flow (if flows weaken, anoxic zones move upstream and vice versa) (Thornton, 1990). Lateral variation is most likely to occur in Kinrara Lake, given the single source, spring-fed nature and modern-day lateral variation in macrophytic communities, with clearly higher macrophytic abundance in the upper-freshwaters transitioning to barren waters lacking substrate and life other than microbial biofilms in the areas toward the downstream lake sill.

Endogenic carbonate is represented by Ca/∑Fe, Ti, Al, as used by Mueller et al. (2009) as an environmental proxy for aridity. This is based on the formation of evaporitic carbonate deposits reflecting a lower precipitation/evaporation (P/E) ratio. While evaporative concentration is not the primary mode of carbonate precipitation in the Kinrara record, drier conditions and steady inflows with minimal disturbances (e.g. flood events and cyclones) are still required for microbially mediated carbonate supersaturation, whether they be microbial biofilms of cyanobacterial blooms. Therefore, the use of this ratio as an aridity proxy is appropriate for this study.

5.3. Interpretation of Kinrara Lake $\delta^{18}O$ record

In lacustrine sediments, stratigraphic changes in the $\delta^{18}O$ values of primary carbonates can reflect fluctuation of changes in temperature, P/E, changes in the isotopic composition of precipitation (δp), or combinations of all of these (Leng and Marshall, 2004). The factor that dominates the $\delta^{18}O$ value is determined by climate and physical lake characteristics affecting lake water balance. As Kinrara Lake is a small, spring-fed, open, low-latitude lake in a hot semi-arid climate (Köppen Climate Classification - Peel et al., 2007), changes in carbonate $\delta^{18}O$ values in the sedimentary record are likely to reflect changes in both water balance and temperature. Despite modern carbonate $\delta^{18}O$ values being in equilibrium with the observed $\delta^{18}O$ value of modern lake water (Table S2) at the measured temperature of 27 °C (SI - Section 4), it is unlikely that changes in $\delta^{18}O$ values in the past are due to temperature effects alone, as these are likely to have been only 1–2 °C over the course of the Holocene (Li et al., 2023).

In monsoonal climates, average δp is controlled by changes in the proportion of intense monsoonal or cyclonic rainfall with low δp and trade wind derived rainfall with high δp (Zwart et al., 2018; Munksgaard et al., 2019; Bird et al., 2020). In seasonally dry, low-latitude lacustrine environments, dry periods exaggerate the range of this signal due to evaporative enrichment of heavier isotopes in lake waters at times of low precipitation (Fan et al., 2018; Leng and Marshall, 2004; Tanner, 2010; van Hardenbroek et al., 2018a; Bird et al., 2019). Evaporative enrichment is evident in modern Kinrara Lake water, as shown by an increase in $\delta^{18}O$ values of 1.5 ‰ during the dry season (Table S2) and this effect is apparent in the carbonate isotope records.

Periods of high rainfall not only lead to more negative $\delta^{18}O$ values (supported by an increase in lithogenic elements in the ITRAX record), but also to dilution of lake waters resulting in conditions not suitable for endogenic carbonate precipitation. The absence of endogenic carbonates in the mid-Holocene, coupled with a loss of mollusc communities strongly suggest that the mid-Holocene was a time of relatively high precipitation (Fig. 12). Kinara Lake is a potentially open system, as a ~1 m increase in water level over modern levels will overtop the Kinrara Basalt dam wall, allowing water to discharge directly into Glenofty Creek. Greater volumes of water will flush accumulated cations from the lake thereby creating unsuitable conditions for either gastropod or

endogenic carbonate precipitation.

As groundwater is the primary perennial source of water to Kinrara Lake, it is important to consider how this will influence the $\delta^{18}O$ value of lake waters. Groundwater values generally reflect mean weighted precipitation over long, at least multi-annual and more likely decadal, time periods (Leng and Marshall, 2004). In semi-arid seasonal environments, groundwater recharge tends to be dominated by the wet-season $\delta^{18}O$ value, derived from high rainfall events (Eastoe and Dettman, 2016). Therefore, the shallow freshwater aquifers in the McBride Province feeding Kinrara Lake are likely to reflect mean δp over the greater catchment area (~7.7 ‰; Table S2).

Elemental abundances and ratios (Ti, Rb, Fe/Mn and Inc./Coh) and a sharp increase in macrofossils in the sedimentary profile at the sharp contact between Unit 4 early-Holocene carbonate marls and Unit 3 organic-rich mud, both indicate an abrupt transition to wetter than modern conditions at ~8200 cal yr BP, as the lake level overtopped the sill. Carbonate $\delta^{18}O$ values show a slight lag with values abruptly decreasing by ~1 ‰ by ~7800 cal yr BP followed by little to no carbonate (endogenic or biogenic) precipitation throughout the mid-Holocene. One possibility for this lag is that $\delta^{18}O$ values reflect higher effective precipitation on a groundwater-basin scale, thereby requiring a consistently high amount of rainfall to 'dilute' the background isotopic response. In contrast, elemental ratios and sediments reflect a relatively smaller local lake catchment scale and therefore manifest a more immediate change to any local environmental forcing. As $\delta^{13}C$ value also remained constant through the early-Holocene, and conditions still favoured carbonate precipitation and growth of gastropods, it is likely that the transition to wetter conditions was more gradual (over ~1 ka, beginning ~8700 cal yr BP), continuing until rainwater input increased to a point where local rainwater inflows dominated the $\delta^{18}O$ value of the lake water.

Carbonate precipitation becomes abundant again at 2800 cal yr BP, indicating regional drying and lake levels consistently below the sill. The upper range of $\delta^{18}O$ values of all carbonate precipitated from this period toward the present is similar to the last carbonates precipitated in the early-Holocene, but values are more erratic and include short-lived excursions to values that are lower by up to 1.5 ‰, occurring at the beginning or end of a period of no carbonate precipitation. These characteristics suggest that hydroclimate was more variable over this period, and included wet periods of $\delta^{18}O$ value rainfall was occasionally sufficient to flush the lake (~1800 and 500 cal yr BP).

From ~1000 cal yr BP to present, $\delta^{18}O_{bio}$ values are consistently higher than $\delta^{18}O_{endo}$ (by ~ + 1‰). The exact process behind this decoupling is unclear given the present data available (*G. gilberti* $n = 7$, *M. tuberculata* $n = 7$). If lake conditions were in isotopic equilibrium with local temperature, as they are in the present system (Supplementary Information Section 4), this could be due to $\delta^{18}O_{bio}$ values reflecting a cooler benthic environment relative to the upper water layers (Leng and Marshall, 2004). However, amount effects on rainfall $\delta^{18}O$ value generally increase with intensified seasonality as seen during this period. If the lake water is not in equilibrium with temperature, perhaps the gastropods are reflecting seasonal growth in evaporatively ^{18}O-enriched water. Higher resolution sampling over this interval and longer-term modern lake calibration studies are required to determine how the gastropods and endogenic carbonates respond on shorter inter- and intra-annual time scales.

5.4. Interpretation of Kinrara Lake $\delta^{13}C$ record

The $\delta^{13}C_{endo}$ values provide insight into the dynamics of carbon cycling within lakes as a measure of the isotope composition of dissolved inorganic carbon (DIC, mostly HCO_3^-; Leng and Marshall, 2004). Unlike oxygen, no single carbon reservoir dominates the carbon budget of the lake and therefore the $\delta^{13}C$ value of the carbonates potentially represents a number of sources and fractionation processes. There are three dominant processes which influence the carbon composition of DIC in natural waters; 1) the isotope composition of spring/groundwater, 2) CO_2 exchange between the atmosphere and lake water, and 3) photosynthesis/respiration/decomposition of aquatic plants (Leng and Marshall, 2004).

Groundwaters and river waters typically have low $\delta^{13}C_{DIC}$ values (−15 to −10 ‰) (Andrews et al., 1993). However, modern Kinrara spring has values lower than this (−16.7 to −17.2 ‰) (Table S2). This is possibly due to CO_2 with a low $\delta^{13}C$ value being incorporated into the DIC pool from decay of low ^{13}C terrestrial organic matter (O'Sullivan and Reynolds, 2004).

Much of the lake record reflects much lower $\delta^{13}C_{endo}$ values than the modern Kinrara lake values, though higher than the measured modern spring values ($\delta^{13}C_{endo}$ mean − 13.3 ‰ in the early-Holocene and − 16.1 ‰ from mid-Holocene to present). These values are similar to $\delta^{13}C$ values that result from photosynthesis/respiration associated with high productivity lake waters. Phytoplankton and macrophytes preferentially uptake ^{12}C from HCO_3^- during photosynthesis, resulting in relatively higher $\delta^{13}C$ values in precipitated carbonate (−19 to −7.5‰) due to eplimnetic ^{12}C-depletion, or 'drawdown' of pCO_2 (Leng and Marshall, 2004; O'Sullivan and Reynolds, 2004). However, the values in the record still fall in the range of those expected from soil respiration entrained into the water, making exact apportionment between sources difficult. Equilibration of DIC with pCO_2 occurs even without the influence of organisms in lakes (Usdowski and Hoefs, 1990). When lake water DIC comes to equilibrium with pCO_2 (which is usually −8‰ to −7‰), $\delta^{13}C$ values move toward +1‰ to +3‰ and with more alkaline conditions favouring $CO_{3(aq)}^{2-}$ DIC species, however, this only occurs in closed basins with very high E/P (Usdowski and Hoefs, 1990).

High $\delta^{13}C_{endo}$ values (+3.4 ‰) at 10500 cal yr BP (at the beginning of the massive endogenic carbonate precipitation phase) likely reflects CO_2 from volcanic degassing entering groundwater, associated with the Kinrara eruption. Similar values have been reported from other low-latitude arid lakes in volcanically active regions such as the Ethiopian Rift Valley, Lake Kivu (Votava et al., 2017) and Lake Langano Basin (Main Ethiopian Rift) also Laguna Seca in the Chilean Altiplano Tropics (Schwalb et al., 1999) all of which have been attributed to volcanic activity, rather than pCO_2 equilibration.

5.5. Kinrara lake paleohydrology

5.5.1. Early-Holocene (10,500 to 8200 cal yr BP)

The early-Holocene in tropical Australia is generally characterised as incorporating a transition from the drier glacial conditions of the late Pleistocene toward relatively wetter conditions, though still remaining relatively drier than the mid-Holocene (Reeves et al., 2013a; Reeves et al., 2013b). Foraminifera Mg/Ca estimates of sea surface temperature (SST) indicate that the early-Holocene was the warmest period during the last 30 ka, with SSTs 0.5–1 °C higher in the Pacific (Stott et al., 2004; Visser et al., 2003; Xu et al., 2010). This is coupled with the highest rate of terrigenous sedimentation on the Great Barrier Reef, reflecting increased precipitation and extensive catchment erosion from 13 to 8 ka (Hughes and Croke, 2017; Lewis et al., 2013). Maximum $\delta^{18}O$ values in a speleothem from Chillagoe Cave (Fig. 1 for location) occur at 11 ka and decrease progressively to 8 ka, also indicating a progressive shift from drier toward wetter conditions (Turney et al., 2006a).

Generally, Wet Tropics pollen records (Fig. 1) show a gradual transition into wetter conditions with continuing expansion of woody and/or rainforest taxa throughout the early-Holocene (Haberle, 2005; Moss and Kershaw, 2007; Walker, 2007). Gradual increases in precipitation are also suggested for Bromfield Swamp (Burrows et al., 2016) initiating at ~10 ka and plateauing at ~8.5 ka. However, this is not consistent throughout the Australian tropics with some sites experiencing localised drying or pronounced wetter events in this time period (Muller et al., 2008; Reeves et al., 2013b; Tibby and Haberle, 2007).

The Kinrara Lake record suggests stable drier-than-modern conditions pertained at the initiation of lake sedimentation (10.5 ka) with an

initially gradual change toward wetter conditions from 8.5 ka. This period included short-lived more arid periods centred on 10.3 and 9.7 ka and was followed by an abrupt shift to a consistently significantly wetter than modern climate at 8.2 ka. At this time there is a large concentration of gastropods in the record (over 3 cm) marking an abrupt transition also reflected in other geochemical proxies (increasing Ti, Rb, Fe/Mn, Inc./Coh) that are suggestive of an increase in precipitation associated with an increase in monsoon activity. This transition marks the end of the early carbonate phase, suggesting a sustained switch to higher monsoon rainfall, with sustained higher seasonal rainfall and overall effective precipitation. This in turn led to at least seasonal flushing of the lake over the sill at the southern end of the lake, reducing cation concentrations below that required to sustain carbonate precipitation.

Changes suggestive of a shift to wetter conditions are also seen in pollen and geochemical data at Lynch's Crater at this time, which lasted for about 400 years (Muller et al., 2008; Turney et al., 2004). Wetter conditions after ~8.2 ka correspond with meltwater-induced slowdown of the North Atlantic Thermohaline Circulation and subsequent southward shift of the ITCZ in the ocean basins (Muller et al., 2008). This is coupled with an expansion of the western boundary of the IPWP (Linsley et al., 2010; Reeves et al., 2013a) with low $\delta^{18}O$ values in speleothems localised to South China and Flores, but not Borneo, reflecting a southward movement of the ITCZ (Reeves et al., 2013b). Gradual transitions to monsoon conditions have also been linked to a minimum in Southern Hemisphere insolation that reduced seasonality (Haberle, 2005).

5.5.2. Mid-Holocene (8.2 to 4.2 ka)

The mid-Holocene marks broad Australian trends to higher land surface temperatures (e.g. Li et al., 2023), peak SSTs (Linsley et al., 2010; Tachikawa et al., 2009) and increased precipitation related to a sea-level highstand at that time (Hughes and Croke, 2017; Lewis et al., 2013; Reeves et al., 2013b). The monsoon was very active with a southward movement of the ITCZ (Reeves et al., 2013a). Peak monsoon conditions are also reflected in the Wet Tropics more broadly. Bromfield Swamp experienced higher than modern precipitation (Burrows et al., 2016) while rainforests reached their maximum extent, based on ODP 820 (Moss and Kershaw, 2007) and lake microfossil records; Euramoo (Haberle, 2005), Barrine (Walker, 2007; Li et al., 2022). The Witherspoon Swamp pollen record, from the savannas north of Kinrara, is also interpreted as indicating a wetter-than-modern mid-Holocene (Moss et al., 2012),

In the Kinrara Lake record, an and almost total absence of carbonate precipitation and an indication of increased precipitation derived from Ti, Rb, Fe/Mn characterises the mid-Holocene. Two potentially drier periods are indicated by some carbonate precipitation (7.9 and 6.9 ka) reflecting times when rainfall was insufficient to consistently lead to overtopping of the lake sill, and flushing of the lake basin. These events were short-lived (for 300 and 60 years, respectively, as indicated by the ITRAX Ca record, Fig. 6). These minor drying phases correspond with a weak warm ENSO phase (7–4 ka), inferred from humification and pollen records (Turney et al., 2006b), further supported by a contraction of the IPWP inferred from coral records (1–2 °C at south western and south eastern edges of the IPWP) suggesting the existence of cooler and drier intervals in this period (Abram et al., 2009). Fossil corals from the south eastern IPWP and the Coral Sea at this time also suggest less frequent, and less extreme, El Niño events compared with today (Abram et al., 2009; Corrège et al., 2000; Gagan et al., 2004; McGregor and Gagan, 2004; Tudhope et al., 2001).

5.5.3. Late-Holocene (4.2 ka to present)

The late-Holocene in northern Australia marks a period of greater climatic variability associated with the intensification (i.e. increased amplitude) of ENSO (Donders et al., 2007), with more intense arid events associated with the El Niño mode (Reeves et al., 2013a). This trend is also reflected regionally across the Wet Tropics and the surrounding seasonal tropics. Proxy data from Lakes Euramoo and Barrine suggest an increase in taxa more resilient to climatic extremes (Haberle, 2005; Walker, 2007; Li et al., 2022). A decline in lake level at Euramoo (Tibby and Haberle, 2007) is also indicative of an intensification of ENSO at this time. Higher resolution studies suggest wet-dry cycles and abrupt climatic changes occur at Bromfield Swamp (Burrows et al., 2014; Burrows et al., 2016) which corresponds to the 1000–2000 year ENSO cycle seen at Lynch's Crater (Turney et al., 2004) and also seen within corals in the western Pacific (McGregor and Gagan, 2004). The Witherspoon Swamp pollen record is also interpreted as indicating a return to drier conditions similar present with increased climate variability after ~2 ka BP (Moss et al., 2012).

The Kinrara record corroborates these regional trends, enabling a more precise estimate of 2.8 ka for the transition into a period of more variable hydrological regime in the late-Holocene, with an overall trend to average drier conditions toward the present, but also interspersed with significant centennial-scale relatively extreme wet periods. Endogenic (aragonite photosynthetic/evapo-conentrative precipitates) and biogenic carbonates reappear at 2.8 ka, though in lower amounts than in the early-Holocene. These carbonates are characterised by substantial variation in $\delta^{18}O_{endo}$ values (−8.5 to −13.3 ‰) further supporting the overall interpretation of greater climatic variability during this period.

The lowest $\delta^{18}O$ values in the record occur between 1.8 and 1.5 ka suggesting a brief period of intensified precipitation associated with strengthening of monsoon conditions, with other more brief periods of low values centred on 2.7 and 0.7 ka. The short-lived nature of these events may also indicate periods of increased cyclonic activity on a regional scale as geochemical data within the lake does not suggest increased detrital input. Tropical cyclones produce precipitation with $\delta^{18}O$ values (<−10 ‰), significantly lower than average monsoonal precipitation (Haig et al., 2014; Munksgaard et al., 2019; Zwart et al., 2018). From 1.6 to 1.1 ka, $\delta^{18}O_{endo}$ values increase by ~1 ‰ and other geochemical proxies also indicate a period of drying. Thereafter $\delta^{18}O_{endo}$ values decrease gradually, reaching a minimum at ~0.3 ka, before gradually increasing again into present values (−11 ‰). This minimum and subsequent increase is also recorded in $\delta^{18}O$ values from a Chillagoe speleothem (beginning 0.8 ka), with the minimum at 0.4–0.22 ka, interpreted as indicating maximum cyclonic activity, before transitioning into a relatively stable present period (Haig et al., 2014).

6. Conclusions

The Kinrara record is relatively unique in northern Australia and the tropics more generally, in that an association with volcanism not only formed the lake, but also provided the continuous supply of high-DIC water to maintain a perennial shallow lake in a highly seasonal environment, one that contains a semi-continuous record of carbonate precipitation. Multiproxy geochemical and stable isotope analysis of carbonates in this study provides novel insight into the hydrodynamics of a seasonally dry tropical site in north eastern Australia throughout the Holocene.

The Kinrara record appears to reflect trends similar to those identified throughout the wet tropics, with pronounced limnological responses to hydrologic and climatic shifts represented in the core. The geochemical and sedimentological characteristics of Kinara Lake record highlights three distinct paleohydrological phases over the last ~10.5 ka; (1) a relatively stable drier-than-modern phase during the early-Holocene (10.6–8.2 ka); (2) an abrupt shift wetter-than-modern monsoon-dominated conditions throughout the mid-Holocene and extending into the late-Holocene (8.2–2.8 ka), and (3) a most recent phase from 2.8 ka to the present, characterised by an overall drying trend overlain by increased variability likely due to increased intensity of ENSO related monsoon variability.

Within the broad trends recorded in the record it is possible to identify short-lived relatively abrupt transitions and anomalies. An anomalously high carbon isotope value at the beginning of carbonate

deposition at 10.5 ka likely reflects a major influx of volcanogenic CO_2 that initiated abundant carbonate precipitation over the next 2.3 ka. A mass gastropod mortality event at 8.8 ka, potentially reflects a time at which rainfall briefly increased to the point where the lake became consistently flushed and shell calcification was not possible, with carbonate deposition ceasing completely after a further increase in rainfall after 8.2 ka. Brief periods of carbonate precipitation at 7.8 ka and 6.9 ka during the overall wetter-than-modern mid-Holocene likely represent distinct drought events that led to the lake not being flushed of spring-derived DIC. Brief periods of low ^{18}O carbonate precipitation in the last 2.8 ka potentially represent times of increased cyclonic activity in the region, during a period characterised by increased ENSO related variability. Further calibration studies and other paleoenvironmental analyses within the Kinrara archive will hopefully corroborate these findings or provide further insight into the savanna dynamics within a sub-tropical climate.

CRediT authorship contribution statement

Julie James: Conceptualization, Formal analysis, Investigation, Methodology, Validation, Visualization, Writing – original draft. **Rainy Comley:** Formal analysis, Investigation, Methodology, Visualization, Writing – original draft. **Christopher M. Wurster**: Conceptualization, Investigation, Methodology, Writing - original draft. **Vladimir Levchenko:** Formal analysis, Investigation, Methodology, Writing – original draft. **Patricia Gadd:** Formal analysis, Investigation, Methodology, Visualization, Writing – original draft. **Michael I. Bird:** Conceptualization, Data curation, Formal analysis, Funding acquisition, Investigation, Methodology, Project administration, Supervision, Validation, Visualization, Writing – original draft, Writing – review & editing.

Declaration of Competing Interest

The authors declare that they have no known competing financial interests or personal relationships that could have appeared to influence the work reported in this paper.

Data availability

all data is available in the supplementary material

Acknowledgements

We thank the property owners at Kinrara Station, Shane and Robyn O'Brien, for permission to access the lagoon, as well as Jen Whan, Shane Askew, Brendan Jones and Yi Hu for assistance with the analytical techniques. Stephen Maxwell kindly provided the gastropod species identifications. This research was funded by AINSE award ALNGRA11038, the Australian Research Council Centre of Excellence for Australian Biodiversity and Heritage (CE170100015) and an Australian Research Council Laureate Fellowship to M.I·B (FL140100044).

Appendix A. Supplementary data

Supplementary data to this article can be found online at https://doi.org/10.1016/j.palaeo.2023.111985.

References

Abram, N.J., McGregor, H.V., Gagan, M.K., Hantoro, W.S., Suwargadi, B.W., 2009. Oscillations in the southern extent of the Indo-Pacific warm Pool during the mid-Holocene. Quat. Sci. Rev. 28 (25–26), 2794–2803.

Andrews, J., Riding, R., Dennis, P., 1993. Stable isotopic compositions of recent freshwater cyanobacterial carbonates from the British Isles: local and regional environmental controls. Sedimentology 40 (2), 303–314.

Apolinarska, K., Pełechaty, M., Kossler, A., 2015. Within-sample variability of δ 13 C and δ 18 O values of freshwater gastropod shells and the optimum number of shells to measure per sediment layer in the Paddenluch palaeolacustrine sequence, Germany. J. Paleolimnol. 54 (4), 305–323.

Ascough, P., Bird, M., Brock, F., Higham, T., Meredith, W., Snape, C., Vane, C.H., 2009. Hydropyrolysis as a new tool for radiocarbon pre-treatment and the quantification of black carbon. Quat. Geochronol. 4 (2), 140–147.

Bird, M.I., Levchenko, V., Ascough, P.L., Meredith, W., Wurster, C.M., Williams, A., Apperley, D.C., 2014. The efficiency of charcoal decontamination for radiocarbon dating by three pre-treatments–ABOX, ABA and hypy. Quat. Geochronol. 22, 25–32.

Bird, M.I., Wynn, J.G., Saiz, G., Wurster, C.M., McBeath, A., 2015. The pyrogenic carbon cycle. Annu. Rev. Earth Planet. Sci. 43, 273–298.

Bird, M.I., Brand, M., Diefendorf, A.F., Haig, J.L., Hutley, L.B., Levchenko, V., Ridd, P.V., Rowe, C., Whinney, J., Wurster, C.M., Zwart, C., 2019. Identifying the 'savanna'signature in lacustrine sediments in northern Australia. Quat. Sci. Rev. 203, 233–247.

Bird, M.I., Haig, J., Hadeen, X., Rivera-Araya, M., Wurster, C.M., Zwart, C., 2020. Stable isotope proxy records in tropical terrestrial environments. Palaeogeogr. Palaeoclimatol. Palaeoecol. 538, 109445.

Blaauw, M., Christen, J.A., 2011. Flexible paleoclimate age-depth models using an autoregressive gamma process. Bayesian Anal. 6 (3), 457–474.

Boës, X., Rydberg, J., Martinez-Cortizas, A., Bindler, R., Renberg, I., 2011. Evaluation of conservative lithogenic elements (Ti, Zr, Al, and Rb) to study anthropogenic element enrichments in lake sediments. J. Paleolimnol. 46 (1), 75–87.

BOM, 2019a. Climate data online Mount Surprise Township. Retrieved from. http://www.bom.gov.au/jsp/ncc/cdio/weatherData/av?p_nccObsCode=122&p_display_type=dailyDataFile&p_startYear=1978&p_c=-180618129&p_stn_num=030036.

BOM, 2019b. Monthly Rainfall Craigs Pocket Station. Retrieved from. http://www.bom.gov.au/jsp/ncc/cdio/weatherData/av?p_nccObsCode=139&p_display_type=dataFile&p_startYear=&p_c=&p_stn_num=032082.

Bowen, G.J., 2019. The Online Isotopes in Precipitation Calculator, Version OIPC3.1 (4/2017). Retrieved from. http://www.waterisotopes.org.

Boyle, J., 2002. Inorganic geochemical methods in palaeolimnology. In: Tracking Environmental Change Using Lake Sediments. Springer, pp. 83–141.

Bréhéret, J.G., Fourmont, A., Macaire, J.J., Négrel, P., 2008. Microbially mediated carbonates in the Holocene deposits from Sarlièvre, a small ancient lake of the French Massif Central, testify to the evolution of a restricted environment. Sedimentology 55 (3), 557–578.

Breitenbach, S.F., Bernasconi, S.M., 2011. Carbon and oxygen isotope analysis of small carbonate samples (20 to 100 μg) with a GasBench II preparation device. Rapid Commun. Mass Spectrom. 25 (13), 1910–1914.

Burrows, M.A., Fenner, J., Haberle, S.G., 2014. Humification in Northeast Australia: Dating millennial and centennial scale climate variability in the late-Holocene. The Holocene 24 (12), 1707–1718.

Burrows, M., Heijnis, H., Gadd, P., Haberle, S., 2016. A new late Quaternary palaeohydrological record from the humid tropics of northeastern Australia. Palaeogeogr. Palaeoclimatol. Palaeoecol. 451, 164–182. Retrieved from. https://doi.org/10.1016/j.palaeo.2016.03.003.

Cheng, C., Shao, Z., Vollrath, F., 2008. Silk fibroin-regulated crystallization of calcium carbonate. Adv. Funct. Mater. 18 (15), 2172–2179.

Cohen, B.E., Mark, D.F., Fallon, S.J., Stephenson, P.J., 2017. Holocene-Neogene volcanism in northeastern Australia: Chronology and eruption history. Quat. Geochronol. 39, 79–91. https://doi.org/10.1016/j.quageo.2017.01.003.

Corrège, T., Delcroix, T., Récy, J., Beck, W., Cabioch, G., Le Cornec, F., 2000. Evidence for stronger El Niño-Southern Oscillation (ENSO) events in a mid-Holocene massive coral. Paleoceanography 15 (4), 465–470.

Corzo, A., Luzon, A., Mayayo, M., Van Bergeijk, S., Mata, P., García de Lomas, J., 2005. Carbonate mineralogy along a biogeochemical gradient in recent lacustrine sediments of Gallocanta Lake (Spain). Geomicrobiol J. 22 (6), 283–298.

Croudace, I.W., Rindby, A., Rothwell, R.G., 2006. ITRAX: description and evaluation of a new multi-function X-ray core scanner. Geol. Soc. Lond. Spec. Publ. 267 (1), 51–63.

Davies, S.J., Lamb, H.F., Roberts, S.J., 2015. Micro-XRF core scanning in palaeolimnology: Recent developments. In: Micro-XRF Studies of Sediment Cores. Springer, pp. 189–226.

Davison, W., 1993. Iron and manganese in lakes. Earth Sci. Rev. 34 (2), 119–163.

Dearing, J., 1999. Holocene environmental change from magnetic proxies in lake sediments. In: Quaternary Climates, Environments and Magnetism, pp. 231–278.

Denniston, R.F., Wyrwoll, K.-H., Asmerom, Y., Polyak, V.J., Humphreys, W.F., Cugley, J., Greaves, E., 2013a. North Atlantic forcing of millennial-scale Indo-Australian monsoon dynamics during the last Glacial period. Quat. Sci. Rev. 72, 159–168.

Denniston, R.F., Wyrwoll, K.-H., Polyak, V.J., Brown, J.R., Asmerom, Y., Wanamaker Jr., A.D., Cleary, D., 2013b. A stalagmite record of Holocene Indonesian–Australian summer monsoon variability from the Australian tropics. Quat. Sci. Rev. 78, 155–168.

Department of Environment and Energy, 2019. Einasleigh Uplands Bioregion. Retrieved from. https://www.environment.gov.au/system/files/resources/a8015c25-4aa2-4833-ad9c-e98d09e2ab52/files/bioregion-einasleigh-uplands.pdf.

Dettman, D.L., Reische, A.K., Lohmann, K.C., 1999. Controls on the stable isotope composition of seasonal growth bands in aragonitic fresh-water bivalves (Unionidae). Geochim. Cosmochim. Acta 63 (7–8), 1049–1057.

Diaz, R.J., Breitburg, D.L., 2009. The hypoxic environment. In: Fish Physiology, vol. 27. Elsevier, pp. 1–23.

Donders, T.H., Haberle, S.G., Hope, G., Wagner, F., Visscher, H., 2007. Pollen evidence for the transition of the Eastern Australian climate system from the post-glacial to the present-day ENSO mode. Quat. Sci. Rev. 26 (11−12), 1621–1637. https://doi.org/10.1016/j.quascirev.2006.11.018.

Dupraz, C., Visscher, P.T., Baumgartner, L., Reid, R., 2004. Microbe–mineral interactions: early carbonate precipitation in a hypersaline lake (Eleuthera Island, Bahamas). Sedimentology 51 (4), 745–765.
Eastoe, C., Dettman, D., 2016. Isotope amount effects in hydrologic and climate reconstructions of monsoon climates: Implications of some long-term data sets for precipitation. Chem. Geol. 430, 78–89.
Falster, G., Delean, S., Tyler, J., 2018. Hydrogen peroxide treatment of natural lake sediment prior to carbon and oxygen stable isotope analysis of calcium carbonate. Geochem. Geophys. Geosyst. 19 (9), 3583–3595. https://doi.org/10.1029/2018GC007575.
Fan, J., Xiao, J., Wen, R., Zhang, S., Huang, Y., Yue, J., Xue, D., 2018. Mineralogy and Carbonate Geochemistry of the Dali Lake Sediments: Implications for Paleohydrological Changes in the East Asian Summer Monsoon Margin during the Holocene. Quaternary International.
Gagan, M.K., Hendy, E.J., Haberle, S.G., Hantoro, W.S., 2004. Post-glacial evolution of the Indo-Pacific warm pool and El Nino-Southern Oscillation. Quat. Int. 118, 127–143.
Gischler, E., Gibson, M.A., Oschmann, W., 2008. Giant holocene freshwater microbialites, laguna bacalar, quintana roo, Mexico. Sedimentology 55 (5), 1293–1309.
Glaubrecht, M., Brinkmann, N., Pöppe, J., 2009. Diversity and disparity 'down under': Systematics, biogeography and reproductive modes of the 'marsupial'freshwater Thiaridae (Caenogastropoda, Cerithioidea) in Australia. Zoosystem. Evol. 85 (2), 199–275.
Griffiths, M.L., Drysdale, R.N., Gagan, M., Zhao, J.-X., Ayliffe, L., Hellstrom, J.C., Cartwright, I., 2009. Increasing Australian–Indonesian monsoon rainfall linked to early-Holocene sea-level rise. Nat. Geosci. 2 (9), 636.
Griffiths, M.L., Drysdale, R.N., Gagan, M.K., Frisia, S., Zhao, J.-X., Ayliffe, L.K., Feng, Y.-X., 2010. Evidence for Holocene changes in Australian–Indonesian monsoon rainfall from stalagmite trace element and stable isotope ratios. Earth Planet. Sci. Lett. 292 (1–2), 27–38.
Haberle, S.G., 2005. A 23,000-yr pollen record from Lake Euramoo, wet tropics of NE Queensland, Australia. Quat. Res. 64 (3), 343–356.
Haberle, S.G., Rule, S., Roberts, P., Heijnis, H., Jacobsen, G., Turney, C., Mooney, S., 2010. Paleofire in the wet tropics of Northeast Queensland, Australia. PAGES News 18 (2), 78–80.
Haberzettl, T., Fey, M., Lücke, A., Maidana, N., Mayr, C., Ohlendorf, C., Zolitschka, B., 2005. Climatically induced lake level changes during the last two millennia as reflected in sediments of Laguna Potrok Aike, southern Patagonia (Santa Cruz, Argentina). J. Paleolimnol. 33 (3), 283–302.
Haig, J., Nott, J., Reichart, G.-J., 2014. Australian tropical cyclone activity lower than at any time over the past 550–1,500 years. Nature 505 (7485), 667.
Hallan, A., 2011. A Study of Molluscs Applied to Palaeoenvironmental Reconstruction of the Gulf of Carpentaria, Australia, and Phylogeny of the Corbulidae (Bivalvia).
van Hardenbroek, M., Chakraborty, A., Davies, K., Harding, P., Heiri, O., Henderson, A., Panizzo, V., 2018a. The stable isotope composition of organic and inorganic fossils in lake sediment records: current understanding, challenges, and future directions. Quat. Sci. Rev. 196, 154–176.
van Hardenbroek, M., Chakraborty, A., Davies, K.L., Harding, P., Heiri, O., Henderson, A. C.G., Wooller, M.J., 2018b. The stable isotope composition of organic and inorganic fossils in lake sediment records: current understanding, challenges, and future directions. Quat. Sci. Rev. 196, 154–176. https://doi.org/10.1016/j.quascirev.2018.08.003.
Hogg, A.G., Heaton, T.J., Hua, Q., Palmer, J.G., Turney, C.S., Southon, J., Bayliss, A., Blackwell, P.G., Boswijk, G., Ramsey, C.B., Pearson, C., 2020. SHCal20 Southern Hemisphere calibration, 0–55,000 years cal BP. Radiocarbon 62 (4), 759–778.
Hughes, K., Croke, J., 2017. How did rivers in the wet tropics (NE Queensland, Australia) respond to climate changes over the past 30 000 years? J. Quat. Sci. 32 (6), 744–759.
Italiano, F., Yuce, G., Uysal, I., Gasparon, M., Morelli, G., 2014. Insights into mantle-type volatiles contribution from dissolved gases in artesian waters of the Great Artesian Basin, Australia. Chem. Geol. 378, 75–88.
Kershaw, A.P., 1976. A late Pleistocene and Holocene pollen diagram from Lynch's Crater, northeastern Queensland, Australia. New Phytol. 77 (2), 469–498.
Kim, S.-T., Mucci, A., Taylor, B.E., 2007. Phosphoric acid fractionation factors for calcite and aragonite between 25 and 75 C: revisited. Chem. Geol. 246 (3–4), 135–146.
Krause, C.E., Gagan, M.K., Dunbar, G.B., Hantoro, W.S., Hellstrom, J.C., Cheng, H., Rifai, H., 2019. Spatio-temporal evolution of Australasian monsoon hydroclimate over the last 40,000 years. Earth Planet. Sci. Lett. 513, 103–112. https://doi.org/10.1016/j.epsl.2019.01.045.
Kylander, M.E., Muller, J., Wüst, R.A.J., Gallagher, K., Garcia-Sanchez, R., Coles, B.J., Weiss, D.J., 2007. Rare earth element and Pb isotope variations in a 52 kyr peat core from Lynch's Crater (NE Queensland, Australia): Proxy development and application to paleoclimate in the Southern Hemisphere. Geochim. Cosmochim. Acta 71 (4), 942–960. https://doi.org/10.1016/j.gca.2006.10.018.
Leng, M.J., Marshall, J.D., 2004. Palaeoclimate interpretation of stable isotope data from lake sediment archives. Quat. Sci. Rev. 23 (7–8), 811–831.
Leng, M.J., Lamb, A.L., Lamb, H.F., Telford, R.J., 1999. Palaeoclimatic implications of isotopic data from modern and early-Holocene shells of the freshwater snail Melanoides tuberculata, from lakes in the Ethiopian Rift Valley. J. Paleolimnol. 21 (1), 97–106.
Lewis, S., LeGrande, A., Kelley, M., Schmidt, G., 2010. Water vapour source impacts on oxygen isotope variability in tropical precipitation during Heinrich events. Clim. Past 6 (3), 325–343.
Lewis, S.E., Sloss, C.R., Murray-Wallace, C.V., Woodroffe, C.D., Smithers, S.G., 2013. Post-glacial Sea-level changes around the Australian margin: a review. Quat. Sci. Rev. 74, 115–138.
Li, T., Wurster, C.M., Haig, J., Zhou, Y., Zwart, C., Ren, J., Comley, R., Munksgaard, N.C., Gadd, P.S., Bird, M.I., 2022. Environmental change inferred from multiple proxies from an 18 cal ka BP sediment record, Lake Barrine, NE Australia. Quat. Sci. Rev. 294, 107751.
Li, T., Comley, R., Zhang, E., Zhou, Y., Zhou, X., Munksgaard, N.C., Zhu, Z., Haig, J., Zheng, F., Bird, M.I., 2023. Paleo-temperature inferred from brGDGTs over the past 18 cal ka BP from Lake Barrine, tropical NE Australia. Quat. Sci. Rev. 310, 108125.
Linsley, B.K., Rosenthal, Y., Oppo, D.W., 2010. Holocene evolution of the Indonesian throughflow and the western Pacific warm pool. Nat. Geosci. 3 (8), 578.
Lough, J., Llewellyn, L., Lewis, S., Turney, C.S., Palmer, J.G., Cook, C., Hogg, A.G., 2014. Evidence for suppressed mid-Holocene northeastern Australian monsoon variability from coral luminescence. Paleoceanography 29 (6), 581–594.
MacLean, L., Tyliszczak, T., Gilbert, P., Zhou, D., Pray, T., Onstott, T.C., Southam, G., 2008. A high-resolution chemical and structural study of framboidal pyrite formed within a low-temperature bacterial biofilm. Geobiology 6 (5), 471–480.
McCormack, J., Nehrke, G., Jöns, N., Immenhauser, A., Kwiecien, O., 2019. Refining the interpretation of lacustrine carbonate isotope records: Implications of a mineralogy-specific Lake Van case study. Chem. Geol. 513, 167–183.
McGregor, H.V., Gagan, M.K., 2004. Western Pacific coral δ18O records of anomalous Holocene variability in the El Niño–Southern Oscillation. Geophys. Res. Lett. 31 (11).
Mishra, A., Placzek, C., Wurster, C., Whitehead, P., 2019. New radiocarbon age constraints for the 120 km-long Toomba flow, North Queensland, Australia. Aust. J. Earth Sci. 66 (1), 71–79.
Moreno, A., Giralt, S., Valero-Garcés, B., Sáez, A., Bao, R., Prego, R., Taberner, C., 2007. A 14 kyr record of the tropical Andes: the Lago Chungará sequence (18 S, northern Chilean Altiplano). Quat. Int. 161 (1), 4–21.
Moss, P.T., Kershaw, P.A., 2000. The last glacial cycle from the humid tropics of northeastern Australia: comparison of a terrestrial and a marine record. Palaeogeogr. Palaeoclimatol. Palaeoecol. 155 (1–2), 155–176.
Moss, P.T., Kershaw, A.P., 2007. A late Quaternary marine palynological record (oxygen isotope stages 1 to 7) for the humid tropics of northeastern Australia based on ODP Site 820. Palaeogeogr. Palaeoclimatol. Palaeoecol. 251 (1), 4–22.
Moss, P.T., Cosgrove, R., Ferrier, A., Haberle, S.G., 2012. Holocene environments of the sclerophyll woodlands of the Wet Tropics of northeastern Australia. In: Peopled Landscapes. Archaeological and Biogeographic Approaches to Landscapes. Terra Australis, 34, pp. 329–341.
Mueller, A.D., Islebe, G.A., Hillesheim, M.B., Grzesik, D.A., Anselmetti, F.S., Ariztegui, D., Venz, K.A., 2009. Climate drying and associated forest decline in the lowlands of northern Guatemala during the late-Holocene. Quat. Res. 71 (2), 133–141.
Muller, J., Kylander, M., Wüst, R.A., Weiss, D., Martinez-Cortizas, A., LeGrande, A.N., Jacobson, G., 2008. Possible evidence for wet Heinrich phases in tropical NE Australia: the Lynch's Crater deposit. Quat. Sci. Rev. 27 (5–6), 468–475.
Muller, J., McManus, J.F., Oppo, D.W., Francois, R., 2012. Strengthening of the Northeast Monsoon over the Flores Sea, Indonesia, at the time of Heinrich event 1. Geology 40 (7), 635–638.
Munksgaard, N.C., Kurita, N., Sánchez-Murillo, R., Ahmed, N., Araguas, L., Balachew, D. L., Bird, M.I., Chakraborty, S., Kien Chinh, N., Cobb, K.M., Ellis, S.A., 2019. Data descriptor: daily observations of stable isotope ratios of rainfall in the tropics. Sci. Rep. 9 (1), 1–7.
Orr, T.J., Wurster, C.M., Levchenko, V., Ascough, P.L., Bird, M.I., 2021. Improved pretreatment method for the isolation and decontamination of pyrogenic carbon for radiocarbon dating using hydrogen pyrolysis. Quat. Geochronol. 61, 101124.
O'Sullivan, P., Reynolds, C., 2004. Paleolimnology. In: O'Sullivan, P.E., Reynolds, C.S. (Eds.), The Lakes Handbook: Limnology and Limnetic Ecology, vol. 1. Blackwell Publishing, Carlton, Victoria 3053, Australia, pp. 609–667.
Partin, J.W., Cobb, K.M., Adkins, J.F., Clark, B., Fernandez, D.P., 2007. Millennial-scale trends in West Pacific warm pool hydrology since the last Glacial Maximum. Nature 449 (7161), 452.
Peel, M.C., Finlayson, B.L., McMahon, T.A., 2007. Updated world map of the Köppen-Geiger climate classification. Hydrol. Earth Syst. Sci. Discuss. 4 (2), 439–473.
Popa, R., Kinkle, B.K., Badescu, A., 2004. Pyrite framboids as biomarkers for iron-sulfur systems. Geomicrobiol J. 21 (3), 193–206.
QPWS Enhanced Fire Managment Team, 2012. Planned Burn Guidelines: Einasleigh Uplands Bioregion of Queensland. 41. The State of Queenslan, George Street, Brisbane Qld 400.
Queensland Government, 2019. Water monitoring information portal: 120123A (Burdekin River at Valley of Lagoons). Retrieved from. https://water-monitoring.information.qld.gov.au/.
Reeves, J.M., Barrows, T.T., Cohen, T.J., Kiem, A.S., Bostock, H.C., Fitzsimmons, K.E., Petherick, L., 2013a. Climate variability over the last 35,000 years recorded in marine and terrestrial archives in the Australian region: an OZ-INTIMATE compilation. Quat. Sci. Rev. 74, 21–34.
Reeves, J.M., Bostock, H.C., Ayliffe, L.K., Barrows, T.T., De Deckker, P., Devriendt, L.S., Gagan, M.K., 2013b. Palaeoenvironmental change in tropical Australasia over the last 30,000 years–a synthesis by the OZ-INTIMATE group. Quat. Sci. Rev. 74, 97–114.
Rozanov, A.Y., Astafieva, M.M., Hoover, R.B., 2007. Early Proterozoic (2.04 GA) phosphorites of Pechenga Greenstone Belt and their origin. In: Paper Presented at the Instruments, Methods, and Missions for Astrobiology X.
Schultze-Lam, S., Schultze-Lam, S., Beveridge, T.J., Des Marais, D.J., 1997. Whiting events: biogenic origin due to the photosynthetic activity of cyanobacterial picoplankton. Limnol. Oceanogr. 42 (1), 133–141.
Schwalb, A., Burns, S.J., Kelts, K., 1999. Holocene environments from stable isotope stratigraphy of ostracods and authigenic carbonate in Chilean Altiplano Lagoons.

Palaeogeogr. Palaeoclimatol. Palaeoecol. 148 (1), 153–168. https://doi.org/10.1016/S0031-0182(98)00181-3.
Shanahan, T.M., Pigati, J.S., Dettman, D.L., Quade, J., 2005. Isotopic variability in the aragonite shells of freshwater gastropods living in springs with nearly constant temperature and isotopic composition. Geochim. Cosmochim. Acta 69 (16), 3949–3966.
Stott, L., Cannariato, K., Thunell, R., Haug, G.H., Koutavas, A., Lund, S., 2004. Decline of surface temperature and salinity in the western tropical Pacific Ocean in the Holocene epoch. Nature 431 (7004), 56.
Tachikawa, K., Vidal, L., Sonzogni, C., Bard, E., 2009. Glacial/interglacial sea surface temperature changes in the Southwest Pacific Ocean over the past 360 ka. Quat. Sci. Rev. 28 (13–14), 1160–1170.
Tanner, L.H., 2010. Continental carbonates as indicators of paleoclimate. Dev. Sedimentol. 62, 179–214.
Thompson, J.B., 2000. Microbial whitings. In: Microbial Sediments. Springer, pp. 250–260.
Thompson, J., Ferris, F., 1990. Cyanobacterial precipitation of gypsum, calcite, and magnesite from natural alkaline lake water. Geology 18 (10), 995–998.
Thornton, K.W., 1990. Perspectives on reservoir limnology. In: Reservoir Limnology: Ecological Perspectives. John Wiley & Sons, New York, pp. 1–13, 10 fig, 1 tab, 20 ref.
Tibby, J., Haberle, S.G., 2007. A late glacial to present diatom record from Lake Euramoo, wet tropics of Queensland, Australia. Palaeogeogr. Palaeoclimatol. Palaeoecol. 251 (1), 46–56. https://doi.org/10.1016/j.palaeo.2007.02.017.
Tudhope, A.W., Chilcott, C.P., McCulloch, M.T., Cook, E.R., Chappell, J., Ellam, R.M., Shimmield, G.B., 2001. Variability in the El Niño-Southern Oscillation through a glacial-interglacial cycle. Science 291 (5508), 1511–1517.
Turney, C.S., Kershaw, A.P., Clemens, S.C., Branch, N., Moss, P.T., Fifield, L.K., 2004. Millennial and orbital variations of El Nino/Southern Oscillation and high-latitude climate in the last glacial period. Nature 428 (6980), 306.
Turney, C.S., Haberle, S., Fink, D., Kershaw, A.P., Barbetti, M., Barrows, T., Hesse, P., 2006a. Integration of ice-core, marine and terrestrial records for the Australian last Glacial Maximum and termination: a contribution from the OZ INTIMATE group. J. Quat. Sci. 21 (7), 751–761.
Turney, C.S., Kershaw, A.P., Lowe, J.J., van der Kaars, S., Johnston, R., Rule, S., McGlone, M.S., 2006b. Climatic variability in the Southwest Pacific during the last termination (20–10 kyr BP). Quat. Sci. Rev. 25 (9–10), 886–903.
Usdowski, E., Hoefs, J., 1990. Kinetic 13C12C and 18O16O effects upon dissolution and outgassing of CO2 in the system CO2 H2O. Chem. Geol. 80 (2), 109–118.
Visser, K., Thunell, R., Stott, L., 2003. Magnitude and timing of temperature change in the Indo-Pacific warm pool during deglaciation. Nature 421 (6919), 152.
Vogler, R., Núñez, V., Gregoric, D.G., Beltramino, A., Peso, J., 2012. Melanoides tuberculata: the history of an invader. In: Snails: Biology, Ecology and Conservation, pp. 65–84.
Votava, J.E., Johnson, T.C., Hecky, R.E., 2017. Holocene carbonate record of Lake Kivu reflects the history of hydrothermal activity. Proc. Natl. Acad. Sci. 114 (2), 251–256.
Walker, D., 2007. Holocene sediments of Lake Barrine, north-East Australia, and their implications for the history of lake and catchment environments. Palaeogeogr. Palaeoclimatol. Palaeoecol. 251 (1), 57–82. https://doi.org/10.1016/j.palaeo.2007.02.025.
Westall, F., Rincé, Y., 1994. Biofilms, microbial mats and microbe-particle interactions: electron microscope observations from diatomaceous sediments. Sedimentology 41 (1), 147–162.
Wheeler, M.C., Hendon, H.H., Cleland, S., Meinke, H., Donald, A., 2009. Impacts of the Madden–Julian oscillation on Australian rainfall and circulation. J. Clim. 22 (6), 1482–1498.
Whitehead, P.W., 2010. The Regional Context of the McBride Basalt Province and the Formation of the Undara Lava Flows, Tubes, Rises and Depressions.
Wolfe, B.B., Edwards, T.W., Elgood, R.J., Beuning, K.R., 2002. Carbon and oxygen isotope analysis of lake sediment cellulose: Methods and applications. In: Tracking Environmental Change Using Lake Sediments. Springer, pp. 373–400.
Work, K., Mills, C., 2013. Rapid population growth countered high mortality in a demographic study of the invasive snail, Melanoides tuberculata (Müller, 1774), in Florida. Aquat. Invasions 8 (4).
Wright, D.T., 1999. The role of sulphate-reducing bacteria and cyanobacteria in dolomite formation in distal ephemeral lakes of the Coorong region, South Australia. Sediment. Geol. 126 (1–4), 147–157.
Wurster, C.M., Lloyd, J., Goodrick, I., Saiz, G., Bird, M.I., 2012. Quantifying the abundance and stable isotope composition of pyrogenic carbon using hydrogen pyrolysis. Rapid Commun. Mass Spectrom. 26 (23), 2690–2696.
Xu, J., Kuhnt, W., Holbourn, A., Regenberg, M., Andersen, N., 2010. Indo-Pacific warm pool variability during the Holocene and last Glacial Maximum. Paleoceanography 25 (4).
Zwart, C., Munksgaard, N.C., Protat, A., Kurita, N., Lambrinidis, D., Bird, M.I., 2018. The isotopic signature of monsoon conditions, cloud modes, and rainfall type. Hydrol. Process. 32 (15), 2296–2303.